Electronic Supplementary Information: Designing an Innovation System to Support Profitable Electro- and Bio-catalytic Carbon Upgrade

Andrew W. Ruttinger[a], Sakineh Tavakkoli[b], Hao Shen[c], Chao Wang[c], and Sarah M. Jordaan[b,*]

[a] *Robert F. Smith School of Chemical and Biomolecular Engineering, Cornell University, Ithaca, NY, USA, 14853*
[b] *School of Advanced International Studies, Johns Hopkins University, Washington, DC, USA, 20036*
[c] *Department of Chemical and Biomolecular Engineering, Johns Hopkins University, Baltimore, MD, USA, 21218*
[*] *Corresponding author: sarahjordaan@jhu.edu*

Table of Contents

Detailed Process Description

Use of CO_2 as a feedstock presents an opportunity to reduce atmospheric CO_2 concentrations while maintaining production of carbon-based chemicals and fuels. De Luna *et al.* discuss the transformative power of renewably powered electrosynthesis, which presents an attractive step in converting CO_2 to various C1-3 products. [1] A more technical study by Jouny *et al.* evaluated the investment potential for the electrochemical reduction of CO_2 (eCO_2r) to various C1-3 products. [2] Although they do not directly quantify reductions in CO_2 emissions, they highlight the potential for negative emissions when eCO_2r is coupled with renewable energy sources. Formic acid, in particular, is identified as a highly cost competitive product, primarily due to its lower electricity requirements at the electrochemical cell. [2] Methods of synthesis has been well-studied. [3] While market price of formic acid is also high, market size is insufficient for large growth in the annual global production. [2, 4] Conversely,

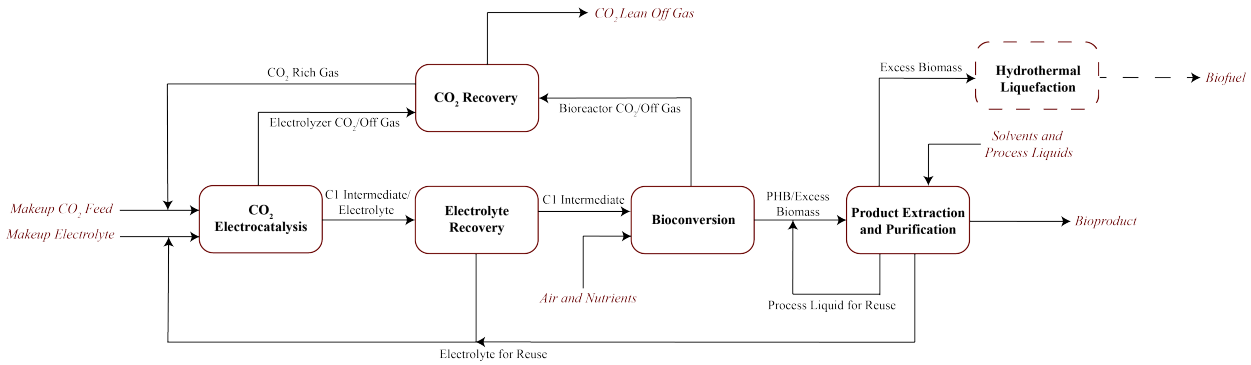

Figure S1: Block flow diagram showing the major subprocesses in our integrated CCU process. The dotted lines denote optional, additional subprocesses.

methanol has the benefit of a large market but suffers from low market price, making penetration through eCO_2r difficult. [2] Upgrade of these carbon intermediates to higher value products through further upstream processing provides an alternative market opportunity.

The integration of eCO_2r with a biocatalytic process is one such process that presents exciting opportunities in the area of CCU. [1, 5, 6] Yishai *et al.* identify formate as a mediator between physicochemical eCO_2r and the biological upgrade to value-added bioproducts. [7] This is primarily due to the efficiency at which electrons are transferred in the eCO_2r.[7, 8, 1, 9] Despite this advantage, during biocatalysis formate is toxic for many metabolites at medium to high concentrations. [10] Co-utilization of formate with other eCO_2r products can help combat this toxicity, while tapping into its high eCO_2r potential. Methanotrophic bacteria such as *Methylobacterium extorquens AM1* have been effective at using methanol as a feedstock for biocatalysis. [11] Importantly, *M. extorquens AM1* is also able to co-utilize formate at lower concentrations.[11, 12] Through bioengineering, *M. extorquens AM1* can be tuned for high selectivity of high value chemical commodities while tolerating the eCO_2r electrolyte. Poly(3-hydroxybutyrate) (PHB) is one example of an attractive product, both for environmental and economic reasons. From an environmental standpoint, PHB is promising due to its properties of biodegradability, biocompatibility, and thermoplasticity, along with its high degree of tune-ability. [13, 14] Furthermore, it has mechanical properties similar to polypropylene. [14] These properties make PHB a good candidate for supplementing current petroleum-based plastic production to reduce plastic waste, which poses a significant threat to ecological diversity and environmental health. [15] From an economic standpoint, PHB has very high market potential with applications ranging from plastic packaging to use in tissue engineering. [14] While commercial manufacturing is expensive, advancements in PHB production technology and scale, volatile oil prices, and increased environmental awareness create a financial opportunity to shift to PHB-based bioplastics. [16]

During biocatalysis, significant waste biomass is produced alongside the desired product, accounting for as high as 85% of the entire microalgae by weight percent. [17] In fact, 100 billion metric tons of biomass waste are generated annually. [18] If disposed of incorrectly, biomass waste can lead to increased GHG emissions. [19] However, this waste biomass has high potential to be processed into high-value products or renewable energy. [19, 20] One such process for biomass transformation is hydrothermal liquefaction (HTL), developed by Pacific Northwest National Laboratory (PNNL) for the renewable generation of biofuel. [21, 22] These biofuels are considered to be a cost-effective and environmentally friendly alternative to petroleum-based products. [19] Integration of this HTL process with the eCO_2r and biocatalysis helps to minimize the amount of waste by-product while reducing GHG emissions and potentially improving process economics. Overall, this integrated approach aims to utilize CO_2 as a feedstock, producing PHB and biomass *via* methanol and formate intermediates.

In order to evaluate the economics of this integrated process, we developed a robust model using Aspen Plus software. [23] Each individual process was also modelled to understand their impact on process economics, highlighting areas for improvement. For a summary of the equipment with key operating parameters, refer to Table S1. Note, the values specified here correspond to the input for the future technology, balanced scenario. The costs of pumps between units was assumed to be negligible in most cases. For cases where a significant pressure increase was necessary, pumps were modelled as centrifugal pump with 80% efficiency. [24]

Electrocatalysis

For the eCO_2r process, we model a gas diffusion electrode (GDE) as the electrolyzer. CO_2 and a buffer solution were fed into the electrochemical cell where CO_2 was reduced at the cathode through the following reactions, depending on the selectivity of the catalyst to formate or methanol:

$$CO_2 + H_2O + 2e^- \longrightarrow HCOO^- + OH^- \quad (1)$$

$$CO_2 + 5H_2O + 6e^- \longrightarrow CH_3OH + 6OH^- \quad (2)$$

Simultaneously, a competing hydrogen evolution reaction took place at the cathode, drawing electrons from the CO_2 electrochemical reduction and reducing the Faradaic efficiency:

$$2H_2O + 2e^- \longrightarrow H_2 + 2OH^- \quad (3)$$

At the anode, the corresponding oxidation reaction occurs:

$$2OH^- \longrightarrow 2e^- + 0.5O_2 + H_2O \quad (4)$$

In the case of the CO_2-to-CH_3OH process, a 1 M potassium bicarbonate ($KHCO_3$) buffer was used. However, for the CO_2-to-$HCOO^-$ process, a 1 M sodium formate (NaHCOO) buffer was used, allowing for cost-effective intermediate recovery. Cobalt phthalocyanine and tin oxide were used as the catalysts for the CO_2-to-CH_3OH and CO_2-to-$HCOO^-$ process, respectively. [25, 26]

Phase separation occurs naturally in the cell, resulting in three outlet streams: an O_2 rich stream leaving the anode, a H_2 rich, unreacted CO_2 stream leaving the cathode, and a formate/methanol enriched electrolyte stream. In order to reduce the waste carbon, the H_2/CO_2 stream undergoes gas separation in a pressure swing absorption (PSA) process which utilizes a porous, CO_2 selective absorbent. PSA is considered the industry standard for large-scale gas separation due to its low energy requirement, reduced environmental impact, and low cost for CO_2 capture. [27, 28, 29, 30] Depending on the configuration, PSA can be operated to achieve over 96% CO_2 purity and 98% CO_2 recovery. [27] Recovered CO_2 is recycled to the electrochemical cell for transformation, while captured H_2 is sent to storage. Costs for PSA gas separation were estimated based on Li *et al.* and their personal communication with Linde. [31] We assume 95 mol% CO_2 purity and 90 mol% CO_2 recovery. [27] Liquid separation is product dependent, due to their physical properties. Separation of methanol and water can be achieved through distillation, producing industry-grade methanol. [32] The 1 M $KHCO_3$ buffer is collected as bottoms in the distillation column, allowing for recycle and reuse through the eCO_2r process. Traditional distillation has proven to be very energy intensive for the purification of formate, as formic acid, resulting in increased emissions and higher costs. [33] This is due to the similar boiling points of formic acid and water. Furthermore, in its formate form, our product would collect in the bottoms of the distillation, along with the buffer, presenting further practical problems. To combat this, we use a 1 M NaHCOO buffer which allows for direct recovery of the product from the electrolyzer and a constant concentration of NaHCOO buffer. Costs for the distillation units were estimated using Aspen Plus. Design is optimized to minimize utility consumption by specifying a low reflux ratio. In the scenario where eCO_2r is integrated with biocatalysis, liquid separation is only necessary to concentrate methanol to 1-5 wt%, reducing both capital and operating costs associated with this step.

Biocatalysis

Formate and methanol enriched electrolyte is fed to the biocatalysis process for further transformation to PHB using *M. extorquens AM1*. Following Levett *et al.*, we employ a two stage, growth and accumulation bioreactor approach. [34] Both were operated at elevated pressure (4 bar) and temperature (38°C) to improve mass transfer of oxygen to the liquid phase. [35] Batch air-lift bioreactors were used to reduce mixing costs and ensure protection of cultures from damage due to shear. [36] For the growth reactor, conditions were phosphorus-rich and ammonia was introduced to stimulate biomass growth. For the accumulation reactor, conditions were phosphorus-deficient to promote PHB growth. [37] PHB was accumulated to 50% of the total biomass present. Dimensions of the bioreactors were estimated based on the required volume, assuming 10% gas holdup and 10% headspace. A height to diameter ratio of 6:1 was used, based on recent specifications from vendors. [38] The overall reactions at the growth and accumulation reactor, respectively, are given as:

$$a\mathrm{CH_3OH} + b\mathrm{HCOO^-} + c\mathrm{NH_3} + d\mathrm{O_2} \longrightarrow e\mathrm{CO_2} + f\mathrm{H_2O} + g\mathrm{C_{3.67}H_{6.4}N_{0.47}O_{2.2}} \quad (5)$$

$$a\mathrm{CH_3OH} + b\mathrm{HCOO^-} + c\mathrm{O_2} \longrightarrow d\mathrm{CO_2} + e\mathrm{H_2O} + f\mathrm{C_4H_6O_2} \quad (6)$$

Stoichiometry of each bioreaction was determined based on current and theoretical yields for conversion of methanol and formate to biomass and PHB. [39] Biomass composition was $C_{3.67}H_{6.4}N_{0.47}O_{2.2}$ [40] based on data from our experimental collaborators and similar to previously reported compositions. [41] Heat generated during bioreactions were estimated based on the heats of combustion for each carbon species. Heat of combustion for biomass and PHB were estimated as -2045 kJ/mol and -1888 kJ/mol, respectively. [34, 42] To maintain reactor conditions, excess heat was removed *via* a coolant fed to the reactor at 5°C and leaving at 20°C. Since the process is very exothermic, each bioreactor requires a cooling jacket and cooling coils. Heat transfer equipment design is based on the process outlined by Levett *et al.* [34] In order to cool the coolant to 5°C a refrigeration cycle is used, assuming a coefficient of performance of 3.[34] Capital expenses for the bioreactors were estimated based on vendor quotes provided by Humbird *et al.*. [38] Additional costs for the cooling coils were estimated through ASPEN Plus by modelling them as a shell and tube heat exchanger.

Oxygen that evolved at the anode during eCO_2r is fed to the bioreactors and is assumed to be at 25°C and 1 atm. The O_2 is compressed using a continuous centrifugal compressor with an isentropic efficiency of 80% and then cooled to reactor temperature using a shell and tube heat exchanger with cooling water fed at 25°C and leaving at 30°C. Capital costs for both were estimated using ASPEN Plus software. O_2 is assumed to leave the reactor at 15% saturation, similar to Levett *et al.* [34]

Biomass and PHB accumulating in the bioreactor can be collected after halting metabolism. Sulphuric acid is used to acidify the biomass at the end of the accumulation period. Then, this broth is sent to a continuous stirred tank reactor where sodium hydroxide neutralizes the acid based on the following stoichiometry and assuming 100% conversion:

$$\mathrm{H_2SO_4} + 2\,\mathrm{NaOH} \longrightarrow \mathrm{Na_2SO_4} + 2\,\mathrm{H_2O} \quad (7)$$

Capital costs were estimated based on recent vendor quotes provided by Humbird *et al.*. [38] The power requirement was determined using the procedure outlined by Chopey in the liquid agitation chapter. [43] Off-gas from the bioreactors were sent to PSA for recovery of CO_2 for recirculation through the eCO_2r process. However, water vapor can lead to reduced absorbent active surface area and therefore, decreased PSA separation efficiency. [27] Therefore, prior to PSA the off-gas is passes through a condenser that reduces the gas temperature to 10°C and liquefies part of the water vapor. A refrigerant is in the condenser to remove heat from the off-gas, with costs estimated using ASPEN Plus.

PHB Extraction and Biomass Treatment

For the downstream processing of biomass and PHB, we follow the process developed by Narasimhan *et al.* and scaled-up by Levett *et al.*, with guidance from industry experts. [44, 34] Upon leaving the neutralization vessel, PHB and biomass were present in the bioreactor effluent at very low concentration (less than 1%). In order to recover PHB from the biomass, the feed must be de-watered to sufficient levels. The biomass is assumed to be 5-20 microns in diameter. [45] First, the bioreactor effluent is sent to a gravity belt thickener where the liquid is thickened to 8 wt% solids content. Capital and operating costs were estimated based on correspondence with a vendor. [46] Next, the thickened sludge was fed to a decanter centrifuge, where the sludge was de-watered to 35 wt% solids. Here, a decanter centrifuge was chosen due to its high capacity and de-watering capabilities. Again, capital and operating costs were estimated using a vendor quote. [47] The inlet and outlet solids concentrations were also selected based on vendor guidance. After de-watering, the wet solids are then fed to a horizontal belt dryer where the solids are dried to 90 wt% solids. For the dryer, ambient air is heated to 100°C using low pressure steam supplied to a shell and tube heat exchanger. Capital and operating costs were estimated using a vendor quote. [48] Once dried, PHB is extracted from the biomass in a batch, pressurized solvent extraction vessel. The dried solids are fed to the vessel with acetone at a acetone to water ratio of 9.[44] The vessel contents are then

heated to a temperature of 90°C, using low pressure steam supplied to a jacket,to ensure PHB remains dissolved in the acetone phase. The vessel is operated at 3 bar. Capital costs were estimated using a vendor quote for a pressure vessel constructed of carbon steel. [49] Operating costs were estimated based on steam requirements to heat the liquid to extraction temperature and stirrer power requirement outlined by Chopey. [43] After sufficient mixing, the effluent is fed to a disk stack centrifuge where the biomass is separated from the hot liquid to 20 wt% solids. Here, a disk stack centrifuge was chosen due to its ability to be operated at elevated temperature and pressure. Capital and operating costs were estimated from literature. [50] PHB lost in the wet biomass effluent must be recovered before collection of the biomass. Therefore, this stream is sent to a rotary drum pressure filter where the biomass can be de-watered to 90 wt%, minimizing the loss of valuable PHB. Due to lack of available public data, outlet solids content was determined from literature based on rotary drum vacuum filters. [51, 52] In order to make the biomass safe for handling, the biomass is washed three times to displace acetone with water. Capital costs were estimated using Matches equipment cost estimates [53] and operating costs were estimated from literature. [50] The biomass is then recovered where it can be sold or upgraded to biofuel through NREL's hydrothermal liquefaction process.[21, 22] The transformation of waste biomass to biofuel through HTL is well-documented, [54] with cost estimates presented in several studies. [21, 22] Recovered PHB-rich liquid is collected and combined with the liquid discharge from the disk stack centrifuge to be processed for PHB recovery.

PHB Recovery

PHB can be extracted from acetone by precipitation with water. First, this PHB-rich liquid is cooled with cooling water in a shell and tube heat exchanger, leaving the heat exchanger at 51°C. The cooled liquid is then sent to a batch stirred vessel, operated at 1 atm. Water is introduced to the vessel in a ratio of 2:1 acetone to water, cooling the liquid to 42°C. [44] The liquid is stirred for 1 hour at a power to volume ratio of 2 kW/m^3 to ensure PHB is effectively precipitated.[44] Capital costs are estimated using a cost vs. capacity plot provided by Harrison. [55] After precipitation, the PHB is present at low concentration. Similar to the biomass treatment process, the PHB is first thickened using a gravity belt thickener, thickened to 8 wt% solids. Next, the thickened sludge is sent to a rotary vacuum drum filter where the PHB is de-watered to 65 wt% solids. The filter is operated at a pressure of 0.5 bar and a filter capacity of 800 $L/m^2.h$ was assumed, based on guidelines from Green and Perry. [56] The PHB is washed with acetone first, to remove any lipids. Then for safe handling, the PHB is washed 3 times to displace acetone with water. Capital and operating costs were estimated using a vendor quote. [57] Finally, the de-watered PHB is fed to a horizontal belt dryer where the solids are dried to 99.5 wt% solids. Again, the air is fed to the dryer *via* a shell and tube heat exchanger, heated with low pressure steam to a dryer inlet temperature of 100°C. The final PHB product is above 99 wt% purity.

Acetone and Water Recovery

Acetone and water leaving the rotary drum pressure filter, gravity belt thickener, and rotary drum vacuum filter are combined and sent for separation and recovery for reuse. First, the liquid is passed through a microfilter where any excess biomass is removed from the liquid to prevent build-up in the distillation column. Microfilters tend to filter particles between 0.1-10 microns, making it ideal for removing biomass. [58] However, any remaining salts present in the liquid will not be filtered. The solid is assumed to be concentrated by a factor of 10. The pressure is increased to 2.5 bar to ensure efficient filtration across the filter. Capital and filter replacement costs were estimated using vendor quotes (-30%/+50%). [59] Power requirement was estimated by the average energy requirement provided by Fasaei *et al.* [50] The acetone and water mixture is sent to a distillation column where the components are separated. Acetone has a boiling point of 56°C, meaning all the acetone leaves the column in the distillate. The distillate is 95 wt% acetone. Capital and operating costs for the distillation column were estimated using ASPEN Plus. [23] The acetone stream, free of any impurities, is mixed with a small acetone makeup feed before it is sent to the extraction vessel, with a small portion being sent to the rotary drum vacuum filter. The water leaving through the bottoms of the distillation column still has salt impurities that need to be removed. Prior to that, the water is cooled by cooling water to 40°C in a shell and tube heat exchanger. Then, the liquid is passed through a nanofiltration unit, which typically filters impurities with a diameter of 0.02-0.2 microns. [58] The filtered salt is assumed to be concentrated by a factor of 10 and the pressure at the entrance to the filter is 3 bar for efficient separation. Capital and filter replacement costs were estimated using a vendor quote (-30%/+50%). [59] Operating costs were estimated based on the power requirements specified by Wafi *et al.* [60] Water leaving the nanofilter is free of impurities. A small makeup water stream is added to the liquid before the water is sent mainly to the precipitation vessel, but also to the rotary drum pressure filter and rotary drum vacuum filter as wash water.

Table S1: Key design parameters for each process unit for the future scenarios.

Process Unit	Process Flow Diagram Label	Design Parameter
Methanol Electrolyzer	ECR-M	Voltage = 2.5 V Current Density = 0.5 A/cm^2 V [1] Faradaic Efficiency = 77.6% [61] Carbon Conversion Efficiency = 80% Catalyst Lifetime = 200 h Catalyst Density = 1.0 mg/cm^2 Temperature = 50°C, Pressure = 1 atm
Formate Electrolyzer	ECR-F	Voltage = 2.5 V Current Density = 0.5 A/cm^2 V [1] Faradaic Efficiency = 97% [62] Carbon Conversion Efficiency = 91% Catalyst Lifetime = 200 h Catalyst Density = 1.0 mg/cm^2 Temperature = 25°C, Pressure = 1 atm
Pressure Swing Adsorption	PSA	Energy Requirement = 561 kJ/kg of CO_2 [27] CO_2 Purity = 95% [27] CO_2 Recovery = 90% [27]
Methanol Distillation Column	DIST-1	Methanol Distillate Concentration < 5 wt% Reflux Ratio = 0.005 Number of Stages = 15 Capacity Limit = 25000 m^3/h
Bottoms Cooler	HE-1	Shell and Tube Heat Exchanger Capacity Limit = 10000 m^3/h Tube Side Fouling Factor = 0.00018 m^{2}K/W Shell Side Fouling Factor = 0.00018 m^{2}K/W Outlet Temperature = 50°C
Air Compressor	C-1	Centrifugal Compressor Isentropic Efficiency = 80% [24] Outlet Pressure = 4 bar
Air Cooler	HE-2	Shell and Tube Heat Exchanger Tube Side Fouling Factor = 0.00035 m^{2}K/W Shell Side Fouling Factor = 0.00018 m^{2}K/W Outlet Temperature = 38°C
Growth Bubble Column Reactor	BIO-R1	Semi-Batch Airlift Bubble Column Reactor Temperature = 38°C, Pressure = 4 bar CH_3OH to Biomass Yield = 0.613 g Biomass/g CH_3OH [39] $HCOO^-$ to Biomass Yield = 0.15 g Biomass/g $HCOO^-$ [39] Maximum Substrate Concentration = 5 wt% [63] Maximum Volume Per Reactor = 800 m^3 Dilution Rate/Growth Rate = 0.2 h^{-1} [64] Batch Time 5.0 h, Empty Time = 40 mins [34] Gas Holdup = 10% [34] Headspace = 10% [34]
Accumulation Bubble Column Reactor	BIO-R2	Batch Airlift Bubble Column Reactor Temperature = 38°C, Pressure = 4 bar CH_3OH to PHB Yield = 0.54 g PHB/g CH_3OH [39] $HCOO^-$ to PHB Yield = 0.13 g PHB/g $HCOO^-$ [39] Maximum Substrate Concentration = 5 wt% [63] Maximum Volume Per Reactor = 800 m^3 Batch Time 5.0 h Gas Holdup = 10% [34] Headspace = 10% [34]

Continued on next page

Process Unit	Process Flow Diagram Label	Design Parameter
Off-Gas Water Condenser	CON-1	Shell and Tube Heat Exchanger Tube Side Fouling Factor = 0.00035 m^2K/W Shell Side Fouling Factor = 0.00018 m^2K/W Outlet Temperature = 10°C
Neutralization Vessel	NEUT	Continuous Stirred Tank Reactor Temperature = 38°C, Pressure = 1 atm Residence Time = 1 h [34] Bulk Velocity = 0.135 m/s [43] Impeller to Tank Diameter Ratio = 0.25 [43] Impeller Efficiency = 85% Maximum Volume Per Reactor = 500 m^3
Biomass Gravity Belt Thickener	GBT-1	Maximum Capacity = 200 m^3/h Inlet Solids Concentration < 1 wt% Outlet Solids Concentration = 8 wt%
Biomass Decanter Centrifuge	CENT-1	Maximum Capacity = 120 m^3/h Inlet Solids Concentration = 8 wt% Outlet Solids Concentration = 35 wt% [34]
Dryer Air Heater	HE-3	Shell and Tube Heat Exchanger Tube Side Fouling Factor = 0.00009 m^2K/W Shell Side Fouling Factor = 0.00035 m^2K/W Outlet Temperature = 100°C [34]
Biomass Horizontal Belt Dryer	DRY-1	Maximum Capacity = 16000 kg/h of Evaporated Water Inlet Solids Concentration = 35 wt% Outlet Solids Concentration = 90 wt% [34]
Solvent Extraction Vessel	SE	Batch Jacketed Stirred Pressure Vessel Temperature = 90°C, Pressure = 3 bar [34] Residence Time = 2 h [34] Bulk Velocity = 0.135 m/s [43] Impeller to Tank Diameter Ratio = 0.25 [43] Impeller Efficiency = 85% Maximum Volume Per Reactor = 50 m^3
Biomass Disk Stack Centrifuge	CENT-2	Maximum Capacity = 120 m^3/h [50] Inlet Solids Concentration = 9.5 wt% Outlet Solids Concentration = 20 wt% [45] Temperature = 90°C, Pressure = 3 bar [34]
Rotary Drum Pressure Filter	P-FILT	Maximum Filter Area = 75 m^2 [53] Inlet Solids Concentration = 20 wt% Outlet Solids Concentration = 90 wt% [51, 52] Temperature = 90°C, Pressure = 3 bar
Acetone Cooler	HE-4	Shell and Tube Heat Exchanger Tube Side Fouling Factor = 0.00018 m^2K/W Shell Side Fouling Factor = 0.00018 m^2K/W Outlet Temperature = 51°C
Precipitation Vessel	PREC	Batch Stirred Vessel Maximum Volume Per Vessel = 150 m^3 Temperature = 42°C, Pressure = 1 atm Residence Time = 1 h [34] Power to Volume Ratio = 2 kW/m^3 [44]
PHB Gravity Belt Thickener	GBT-2	Maximum Capacity = 200 m^3/h Inlet Solids Concentration = 3.5 wt% Outlet Solids Concentration = 8 wt%
Rotary Drum Vacuum Filter	V-FILT	Maximum Filter Area = 75 m^2 Inlet Solids Concentration = 8 wt% Outlet Solids Concentration = 65 wt% [57] Pressure = 0.5 bar [34]

Continued on next page

Process Unit	Process Flow Diagram Label	Design Parameter
Microfilter	MICRO	Filter = 5 μm [45] Pressure = 2.5 bar Concentration Factor = 10 [34] Power Requirement = 1.655 kWh/^{3} [50]
Acetone Distillation Column	DIST-2	Acetone Distillate Concentration = 95 wt% [34] Reflux Ratio = 0.32 [34] Number of Stages = 31 [34] Capacity Limit = 25000 m^3/h
Bottoms Cooler	HE-6	Shell and Tube Heat Exchanger Tube Side Fouling Factor = 0.00018 m^2K/W Shell Side Fouling Factor = 0.00018 m^2K/W Outlet Temperature = 50°C
Nanofilter	NANO	Filter = 0.02 μm [45] Pressure = 3 bar Concentration Factor = 10 [34] Power Requirement = 2.5 kWh/m^3 [60]
PHB Horizontal Belt Dryer	DRY-2	Maximum Capacity = 16000 kg/h of Evaporated Water Inlet Solids Concentration = 65 wt% Outlet Solids Concentration = 99.5 wt% [34]

Assumptions & Scenarios

Major Process Assumptions

While process variables were taken from various sources when possible, in some cases assumptions had to be made to develop a process model. All feedstocks into the process were assumed to be readily available, without impurities, at ambient conditions of 25°C and 1 atm. Air used during the process was also assumed to be available at ambient conditions and at 50% humidity. Cooling water was assumed to be available at 25°C. During electrocatalysis, we simplified the reactions to two competing reactions at the cathode and one oxygen evolution reaction at the anode. Reduction of CO_2 to carbon monoxide (CO) was assumed to be negligible. During pressure swing adsorption, any water vapor remaining in the inlet gas stream was assumed to be low enough that there was no reduction in absorbent performance. It was assumed that no buffer was lost downstream or to build-up during operation.

At the bioreactors, assumption were made based off of the study by Levett *et al.* [34] First, it was assumed that both bioreactors operating with 10% headspace and 10% gas holdup. Volumetric flow rate of the O_2 was assumed to be large enough to provide sufficient mixing for the the bioreactor. Dissolved gas leaving the bioreactors was assumed to be negligible and an O_2 saturation of 15% was assumed. It was assumed growth bioreactors could be emptied in 40 mins. In addition to these assumptions, we assumed all substrate was consumed during biocatalysis. At the growth bioreactor, all substrate was converted to biomass while at the accumulation bioreactor, all substrate was converted to PHB. Although not explicitly modelled, required nutrients for metabolism were assumed to be present in the growth reactor. A summary of these nutrients are giving provided by Levett *et al.* [34] Concentration of the substrates in the bioreactors was assumed to have no effect on growth rate up to a maximum concentration of 5 wt%. At the end of the batch time in the accumulation bioreactor, sulfuric acid was used to halt the metabolism of the microbes. It was assumed that all metabolism was stopped, preventing consumption of PHB. Downstream of the bioreactors, it was assumed that there was 1 % loss of solids at the centrifuges, but none otherwise. At the disk stack centrifuge and the rotary pressure drum filter, three water washes was assumed to displace enough acetone for safe handling of the solids. The rotary vacuum drum filter was assumed to have a filter capacity of 800 L/m^2h, based on state-of-the-art performance described by Perry and Green. [56] During solvent extraction, it was assumed that all PHB was successful extracted and dissolved in the acetone. Similarly, during precipitation all PHB crystallizes and forms particles with a diameter larger than 500 μm, which is reasonable based on the power to volume ratio. [44] During the mirofiltration and nanofiltration processes, we assumed that all biomass and salts, respectively, were filtered, leaving at a concentration factor of 10.

Costs & Financial Assumptions

Along with the process assumptions, financial assumption also had to be made to predict the final net present value (NPV) of the process. First, production was assumed to be at the commercial scale, producing roughly 100,000 tonnes of PHB per year. Due to small adjustments made during development of the model, the actual reference capacity used was 102,748 tonnes/year. Using the same assumption as Jouny *et al.*, our process was operated for 350 days of the year. [2] Our plant life was estimated to be 30 years, with a salvage value of 20% at the end of the plant life. Working capital was estimated to be 5% of the capital investment. To account for depreciation, a 10 year modified accelerated cost recovery system (MACRS) model was used. An interest rate of 10%, compounded annually, was used to estimate NPV. Furthermore, the 2019 US national average income tax rate of 25.7% was used. Based on the U.S. tax system, during years where a negative profit was posted, tax credits equivalent to the profit loss could be carried over into future years. Additionally, tax credits can only be applied to 80% of profit in a given year. All costs were indexed to 2019 USD using Chemical Engineering's Plant Cost Index. [65, 56]

For capital costs, data are compiled from a variety of sources. For the electrolyzers, the price is derived from the sum of individual components. [66] For particular units, ASPEN Plus has robust data on costing and design, allowing us to use purchased costs directly from ASPEN Plus. This pertains to distillation columns, air compressors, pumps, heat exchangers, and knockout drums. For equipment geared towards more specific applications, we consulted vendor for quotes or found literature that provided quotes from vendors. This was done for the remaining units. Individual equipment costs were scaled from the reference values based on scaling factors extracted from Remer and Chai. [67] For the PSA process, the scaling factor was provided by Li *et al.* [31] The required number of operators per unit were estimated by typical labour requirements provided by Ulrich. [68] For the electrolyzer, 10 operators were estimated, based the US Department of Energy H2A analysis for a water electrolysis process. [69] When delivery was not explicitly accounted for in the quote, delivery costs were estiamted to be 5% of the total purchased cost. To determine the final installed cost of the electrolyzer, a Lang factor of 1.67 was used, again based the US Department of Energy H2A analysis for a water electrolysis process. [69] For all other equipment a Lang factor of 4.3 was used based on Perry's recommendation for a solid/liquid chemical plant. [56] For the disk stack centrifuge, piping and instrumentation was included in the quoted price, which was estimated to reduce the factor by 0.4. [56]

Moving to operating costs, maintenance was estimated to be 8% of the total capital costs per year, [56] except for the electrolyzers which was taken as 3% of the total capital costs per year[69] and for equipment where maintenance costs were provided by the vendor. Solid handling costs were estimated to be 10 \$/tonne. [34] Operating labour was calculated assuming operators worked 40 hours per week, leading to 4.5 operators per week per unit, once vacation time and sick days were accounted for. The wages for the chemical plant operators were estimated based on labour statistics from the US Department of Labor indexed to 2019 USD. [70] Supervision, laboratory, and overheads & administration expenses were estimated as 22.5%, 15.0%, and 50.0% of the operating labour, respectively. [56] For equipment, operating costs were estimated based on ASPEN Plus, literature, mathematical calculations, or from vendors, and were scaled linearly to account for capacity.

For feedstock and catalyst prices, current market prices were taken from a variety of sources and indexed to 2019 USD. The prices used in this study and their sources are shown in Table S2. Capture costs for CO_2 were assumed to be \$30/tonne, based on the base case of a the recent study by DeLuna *et al.*. [1] Similarly, process water was estimated to be $\$0.5/m^3$. [34, 56]

Table S2: Feedstock prices used in the present study.

Feedstock	Price (2019 USD/tonne)
Carbon Dioxide	\$30 [2]
Process Water	\$0.502 [34]
Sulfuric Acid	\$200 [56]
Sodium Hydroxide	\$350 [56]
Ammonia	\$250 [71]
Acetone	\$976.6 [72]
Cobalt Phthalocyanine Catalyst	\$1335 [73]
Tin Oxide Nanopowder Catalyst	\$435 [74]
Green Hydrogen Gas (HTL Only)	\$5250 [75]
Blue Hydrogen Gas (HTL Only)	\$2200 [75]
Grey Hydrogen Gas (HTL Only)	\$2050 [75]

Similar to feedstock prices, product market prices were taken through a number of sources and indexed to 2019 USD. Importantly, PHB prices were based on average market prices provided by Levett *et al.* and scaled to 2019 USD. [34] Biomass prices were estimated based on the average minimum selling price determined by NREL. [76] An effective carbon price of 40 $/tonne was used as the baseline, based on the recommendation by economists Stern and Stiglitz to have a CO_2 price of 40-80 $/tonne by 2020. [77] Estimated credits for additional products for separate sub-processes are provided, in addition to the discussed products.

Table S3: Product credits used in the present study.

Product	Credit (2019 USD)
PHB	4482 $/tonne [34]
Biomass	0.51 $/lb [76]
CO_2 Price	40 $/tonne [77]
Methanol	388 $/tonne [78]
Sodium Formate	369 $/tonne [79]
Gasoline	2.69 $/gal [80]
Diesel	3.06 $/gal [80]

Utility prices were an important consideration in the overall plant economics. The costs and operating conditions for each utility are presented in Table S4. Cooling water was assumed to be available at 25°C at a cost of $\$0.057/m^3$. [34, 81] Electricity prices are variable, depending on geographical location and source of electricity. The current OECD average for electricity price is 0.102 $/kWh, while the current US average is 0.065 $/kWh. [82, 83] However, much of those electricity mixes come from CO_2-emitting, non-renewable sources. Prices from renewable sources, particularly photovoltaics (PV) and wind, are considerably lower at 0.045 $/kWh from both sources in 2020. [84] Projections from IRENA show potential pathways for renewable energy to reach 0.02 $/kWh by 2030. [85] For our study, we take a moderate stance, following Haegal *et al.* who map out a 0.03 $/kWh target for renewable electricity. [86] We assume our steam is generated from electricity, meaning our steam price is dependent on this chosen electricity price. We determine a price of 0.022 $/kg, based on the required heat to raise water at ambient conditions to low-pressure steam. For the bioreactor and off gas condenser coolant, we assume a coefficient of performance of 3 leading to a cost of 0.0028 $/MJ of heat removed.

Table S4: Utility prices used in the present study.

Utility	Price (2019 USD)	Inlet Conditions	Outlet Conditions
Cooling Water	0.057 $/m^3 [34]	25°C, 1 atm	30°C, 1 atm
Electricity	0.03 $/kWh [86]	N/A	N/A
Steam	0.022 $/kg	125°C, 2.3 bar (vapor)	125°C, 2.3 bar (liquid)
Bioreactor Coolant	0.0028 $/MJ	5°C, 1 atm	20°C, 1 atm
Condenser Coolant	0.0028 $/MJ	-25°C, 1 atm	-10°C, 1 atm

Finally, while the mass and energy balance were explicitly modelled for our integrated process, leading to economics based on our explicit calculations, a mass and energy balance was not performed explicitly for the HTL process. Instead, economics were estimated by scaling the results of the TEA by Ou *et al.* to our capacity. [22]

Production Scenarios

With all the pieces in place, we evaluate different production scenarios to understand the pathway from our current technology to future, profitable technology. Current data is informed by our experimental collaborators, as well as recent literature. While reported current densities for formate are higher than methanol, we use a single current density value for both products to limit the range of resulting NPVs. Then, we evaluate state-of-the-art technological targets to understand the technological gap we need to overcome. We assume a target value of 200 h for both methanol and formate catalyst lifetime, which fell within the range of values reported in literature. [87] We also investigate how the ratio of substrates influences the NPV. Formate production is highly efficient during eCO_2r, with selectivity above 90%, [1, 7] but is inefficient during biocatalysis. [39] Conversely, methanol is highly efficient during biocatalysis, [39] but suffers from inefficiency during eCO_2r. [9] This inherent technological trade-off presents an opportunity to determine the optimal carbon conversion efficiency and ultimate NPV for an integrated CO_2 upgrade process by varying the substrate composition (Table S6).

Important technological parameters for each scenario are provided in Table S5-S6. We investigate 6 different scenarios for the full process in total. From a technological perspective, we evaluate an integrated process

Table S5: Important process variables for the current and future scenarios investigated in the present work. Sources for each variable are provided.

Process Variable	Current Scenario	Future Scenario
eCO2r CH_3OH Carbon Conversion Efficiency (%)	19.8 (see Electrocatalysis Methods)	80 (est.)
eCO2r CH_3OH Faradaic Efficiency (%)	17.6 (see Fig. S4)	77.6 [61]
eCO2r $HCOO^-$ Carbon Conversion Efficiency (%)	90.1 (see Electrocatalysis Methods)	91 (est.)
eCO2r $HCOO^-$ Faradaic Efficiency (%)	86.7 (see Fig. S5)	97 [62]
eCO2r Current Density (A/cm^2)	0.2 (see Fig. S4-S5)	0.5 [1]
$HCOO^-$ Catalyst Lifetime (h)	100 [62]	200 (est.)
CH_3OH Catalyst Lifetime (h)	50 [88]	200 (est.)
CH_3OH to Biomass Yield (g/g)	0.33 [89]	0.613 [89]
$HCOO^-$ to Biomass Yield (g/g)	0.084 [39]	0.15 [39]
CH_3OH to PHB Yield (g/g)	0.21 [39]	0.54 [39]
$HCOO^-$ to PHB Yield (g/g)	0.027 [39]	0.13 [39]

Table S6: Stoichiometric ratios for the biocatalysis-favouring scenario, balanced scenario, and electrocatalysis-favouring scenario.

Intermediate	Biocatalysis-favouring	Balanced	Electrocatalysis-favouring
CH_3OH	12	4	2
$HCOO^-$	0	20	26

assuming current technology and assuming high efficiency technology for some time in the future. From a substrate perspective, we evaluate three cases of methanol to formate ratios: 1:0, 1:5, and 1:13. From here on, we refer to these scenarios as the biocatalysis-favouring scenario, balanced scenario, and electrocatalysis-favouring scenario, respectively. Bringing these scenarios together, we can understand what the most significant cost drivers and how to reduce overall process costs through technological advancement.

Carbon Footprint Analysis

Alongside economics, determining the carbon footprint to construct, operate, and decommission the proposed process is important for assessing impact. To this end, we create an inventory of CO_2 emissions based on estimates from material, feedstock, and utility usage for each scenario studied. Our reference value for emissions from materials for construction and decommissioning was based on a scaled value from the Ecoinvent database. [90] For our baseline production capacity of 102,748 tonnes of PHB per annum, 292,807 tCO_2eq are generated, or 0.095 $tCO_2eq/tPHB$ over our baseline plant life of 30 years. In the case of feedstocks, reference values for emissions were drawn from literature. Each feedstock, reference value, and its source are provided in Table S7.

Table S7: Process feedstocks and the reference values for emissions. The source of the reference value is provided for each feedstock. All reference values are provided in units of tCO_2 per tonne of feedstock.

Feedstock	Reference Emissions (tCO_2/ tonne of feedstock)	Source
CO_2	-1.0	
Process Water	0.0003276	[91]
Sulfuric Acid	0.00405	[92]
Sodium Hydroxide	1.376	[91]
Ammonia	2.4	[91]
Acetone	2.199	[93]
Cobalt Phthalocyanine, Methanol Catalyst	8.3	[94]
Tin Oxide, Formate Catalyst	17.1	[94]

In addition to feedstocks, consumption of utilities is a major contributor to overall process emissions, particularly if the electricity consumed comes from high emissions intensity sources like hydrocarbon-derived fuels. However, we assume our process is operated by renewable, low emission electricity, which helps reduce the overall emissions. To estimate the emissions intensity of electricity consumption in this process, we use the weighted average of emissions intensity based on global renewable capacity from solar, wind, hydro, and other, which we assume has the same emissions intensity as geothermal electricity generation. [96] Life cycle emissions intensities

Table S8: Renewable electricity global capacity and emissions intensity by renewable source. [95]

Source	Capacity (TWh)	Emissions Intensity (gCO_2eq/kWh)
Hydropower	4222.21	11.6
Wind	1429.62	9.4
Solar	724.09	29.2
Other (Geothermal)	651.81	33.6
Weighted Average		15.01

Table S9: Emissions factors and the units for utilities.

Utility	Reference Emissions	Units
Electricity	15.01	gCO_2eq/kWh
Cooling Water	0.0003276	$tCO_2eq/tonne$
Steam (from Electricity)	0.00904	$tCO_2eq/tonne$
Steam (from Natural Gas)	0.132	$tCO_2eq/tonne$

were estimated based on the median value of harmonized data. [95] Values used in this study are presented in Table S8. Since these estimates represent results from literature published between 1970 and 2010, we anticipate they represent overestimates of life cycle emissions compared to a more decarbonized future.

Cooling water was assumed to have an emission factor equivalent to feedstock process water. Steam is generated from electricity in our baseline scenario, so the emissions are directly related to the emission intensity of electricity generation. An additional emission factor for steam generated from natural gas is provided, based on an emission factor of 0.0548 $kgCO_2eq/ft^3$ provided by the U.S. EPA. [97] All emissions factors are provided in Table S9.

Net emissions for the six scenarios are provided in Table S10. Since the net emissions depends on the source of the CO_2 (*e.g.* point source CO_2 versus direct air capture (DAC) CO_2), an upper and lower bound of net emissions is provided. For all scenarios, we assume a plant capacity of 102,748 tPHB/year and 350 operating days/year. For our more detailed data on the process emissions of each scenario, refer the "Process Emissions" tab in the supplementary spreadsheet accompanying this article.

Table S10: Net emissions for each production scenario studied in the present work. Negative net emissions means more CO_2 is utilized than is emitted, indicating emissions avoided. A range is provided to account for the source of CO_2 used for the PHB production.

Scenario	Net Emissions ($tCO_2/tPHB$)
Biocatalysis-favouring, Current	64.7 - 68.5
Balanced, Current	25.5 - 29.3
Electrocatalysis-favouring, Current	13.6 - 17.5
Biocatalysis-favouring, Future	6.2 - 10.0
Balanced, Future	1.0 - 4.8
Electrocatalysis-favouring, Future	0.08 - 3.9

As expected, the inefficient operation in the current scenarios lead to higher net emissions that lead to excess emissions compared to no PHB production. This is largely a result of high utility requirements, particularly cooling water and steam. The scenario with the least emissions emitted, electrocatalysis-favouring, still emits 13.6 - 17.5 $tCO_2/tPHB$ in excess compared to no operation. These observations are consistent with the economics of the process, where the current scenarios have very poor net present values (see main text).

In future scenarios where favourable operating conditions are met, the net emissions become more promising in some cases. For the biocatalysis-favouring and balanced scenarios, the processes still emit 6.2 - 10.0 and 1.0 - 4.8 $tCO_2/tPHB$, respectively, in comparison to no operation. However, these emission factors are much improved from the three current scenarios. Similar to the economics of the process, emissions are driven by high utility requirements during product separation. As a result, in the electrocatalysis-favouring scenario that has a lower methanol requirement, the process only has net emissions of 0.08 - 3.9 $tCO_2/tPHB$. While the scenario still has net emissions, when compared to the carbon intensity of polypropylene, estimated at 0.94 $kgCO_2eq/kg$-polypropylene, [98], there is a net benefit through product displacement. This improvement in emissions also relates to the economics demonstrated, suggesting reducing usage of utilities is the driver of both improved economics and reduced emissions. However, use of CO_2 removal technologies like DAC is necessary to maximize

avoided emissions. Additional measures like proper PHB disposal (*e.g.* composting, anaerobic digestion) has the potential to further reduce net emissions, although there is significant uncertainty here.

Since an integrated process such as the one presently studied is attractive because of its potential to avoid energy-intensive product separation, we also consider a scenario where we assume the technology is sufficiently matured to by able to bypass this stage. Under these conditions, net emissions are significantly improved at 1.9-5.8, −0.4-3.5, and −1.1-2.7 tCO_2/tPHB for the biocatalysis-favouring, balanced, and electrocatalysis-favouring scenario, respectively. Notably, for both the balanced and electrocatalysis-favouring scenarios there are pathways for avoided upstream emissions. Research efforts towards integration of electrocatalysis and biocatalysis processes without intermediate product separation can play a critical role in both the economic potential and environment impact of such a process.

In terms of gross emissions, at a production capacity of 102,748 tPHB/year, the electrocatalysis-favouring scenarios could generate as low as approximately 8000 tCO_2/year. For the balanced and electrocatalysis-favouring scenarios with processes matured to the point that no product separation is needed, up to 0.04 and 0.12 $MtCO_2$/year could be avoided, respectively. As this technology becomes more efficient and cost-effective, global production capacity should also grow. Currently, PHB production is estimated at 0.1% of polypropylene production, [99] which was estimated at 88.6 million metric tonnes of polypropylene in 2020. [100] Since PHB is considered a good alternative for polypropylene, we can assess the global emission reduction potential for this integrated electrocatalysis and biocatalysis CO_2-to-PHB process as it replaces polypropylene. Here, we plot the annual emissions reduction capacity for the balanced and electrocatalysis-favouring scenarios as a function of total polypropylene production capacity (Fig. S2). We assume all constructed plants have the same production capacity and emissions intensities per tonne of PHB. Our estimates act as a lower bound estimate, since the emissions avoided from any reduction in emissions intensity from feedstock and utilities is not accounted for.

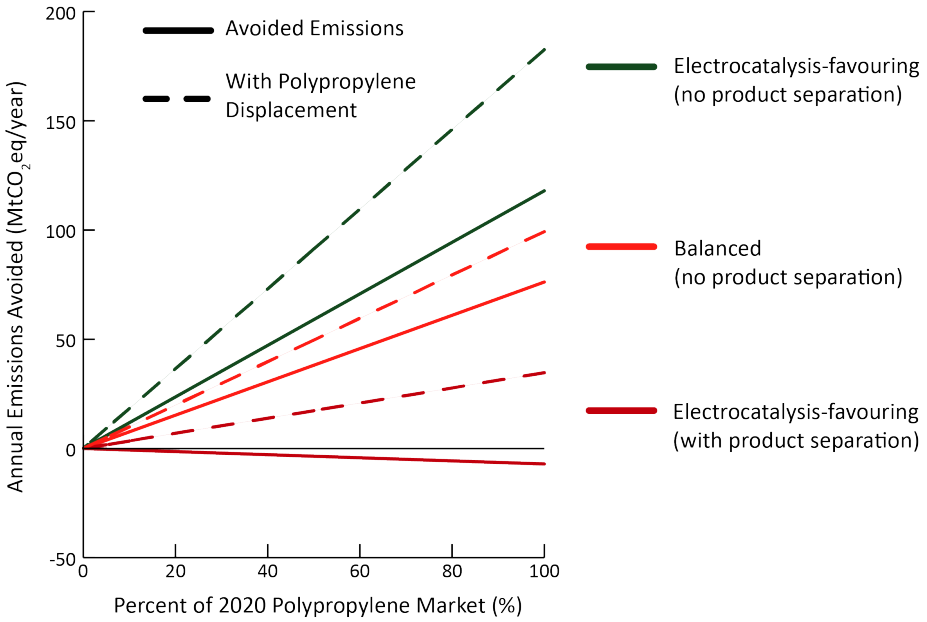

Figure S2: Annual emissions avoided through operation of the proposed integrated electrocatalysis and biocatalysis CCUS process as a function of total 2020 polypropylene market for three selected scenarios. Scenarios are indicated in the legend.

At 10% of the total polypropylene production, 8.9 million metric tonnes per year, PHB production under the balanced and electrocatalysis-favouring scenarios with no product separation could lead to 3.5 and 9.9 $MtCO_2$/year avoided. Accounting for the emissions avoided from substituting polypropylene production, estimated at 0.94 $kgCO_2$eq/kg-polypropylene, [98] an additional 8.3 $MtCO_2$/year would be avoided under all scenarios. Therefore, while the electrocatalysis-favouring scenario with product separation would lead to 0.7 $MtCO_2$/year generated from net emissions, once product displacement is taken into account 7.6 $MtCO_2$/year would be avoided. Reaching 50% market share of polypropylene, the balanced and electrocatalysis-favouring production scenarios with no product separation lead to 34.7 and 50.0 $MtCO_2$ avoided per year. Substitution of polypropylene production would account for another 41.6 $MtCO_2$/year avoided. While such targets are unlikely to be achieved in the near future, as global production systems shifts from petroleum-derived products to renewable or low emission products and economics of CCUS improves, global production capacity of renewable plastics should grow. Our analysis demonstrates both

the economic potential and positive environmental impact of PHB production on a global scale.

Baseline Electrocatalysis Experimental Data

Electrocatalysis Methods

Both the electrochemical reduction of CO_2 to sodium formate and methanol are performed in a three-electrode flow cell system with 1 mol/L sodium bicarbonate as electrolyte. For the CO_2-to-formate conversion, bismuth power (Sigma-Aldrich) was drop-casted onto the gas diffusion electrode (Sigracet 36BB) as working electrode. For the CO_2-to-methanol conversion, a cobalt-phthalocyanine-based nanomaterials was synthesized through a method modified from previous reports [101, 102] as catalysts for working electrode and loaded onto the gas diffusion electrode by spray coating. A saturated calomel electrode was used as reference electrode and IrRuOx-coated titanium screen was used as counter electrode. The working electrode and counter electrode are separated by an anion-exchange membrane(Fumasep-FAA-PK-130) and fed with two electrolyte flows. The tests of CO_2 reduction catalysts performance were performed by using an potentiostat (Metrohm Autolab 302) using a galvanostatic method. During the electroreduction reaction, the gas-phase products were analyzed directly using gas chromatograph-mass spectrometry (GC-MS-QP2010SE Shimadzu), and the liquid products were collected and analyzed by a nuclear magnetic resonance (NMR) spectroscopy (Bruker Fourier 300 MHz). The faradaic efficiencies towards formate and methanol are calculated by the following formulas:

$$FE_{formate}(\%) = \frac{2 \times c_{formate}(mmol/L) \times 96485 \times 100 \times V(L)}{j(mA/cm^2) \times S_{electrode}(cm^2) \times time(sec)} \tag{8}$$

$$FE_{methanol}(\%) = \frac{6 \times c_{methanol}(mmol/L) \times 96485 \times 100 \times V(L)}{j(mA/cm^2) \times S_{electrode}(cm^2) \times time(sec)} \tag{9}$$

where c is the concentration of the product, V is the volume of the liquid, j is the current density, S is the electrode area, and time is the accumulation time of the product.

The carbon conversion efficiencies (CCE) were measured through a flow-rate-controlled experiment using the same electrochemical setup. The CO_2 inlet flow rate was controlled for sufficient conversion of CO_2. The carbon conversion efficiencies towards formate and methanol are calculated by the following formula and the highest CCEs towards formate and methanol are 90.1% and 19.8% respectively.

$$CCE_{formate}(\%) = \frac{c_{formate}(mmol/L) \times V(L)}{Q(mL/min) \times 60 \times time(sec) \times 0.04087(mmol/mL)} \tag{10}$$

$$CCE_{methanol}(\%) = \frac{c_{methanol}(mmol/L) \times V(L)}{Q(mL/min) \times 60 \times time(sec) \times 0.04087(mmol/mL)} \tag{11}$$

Electrolyzer Cell

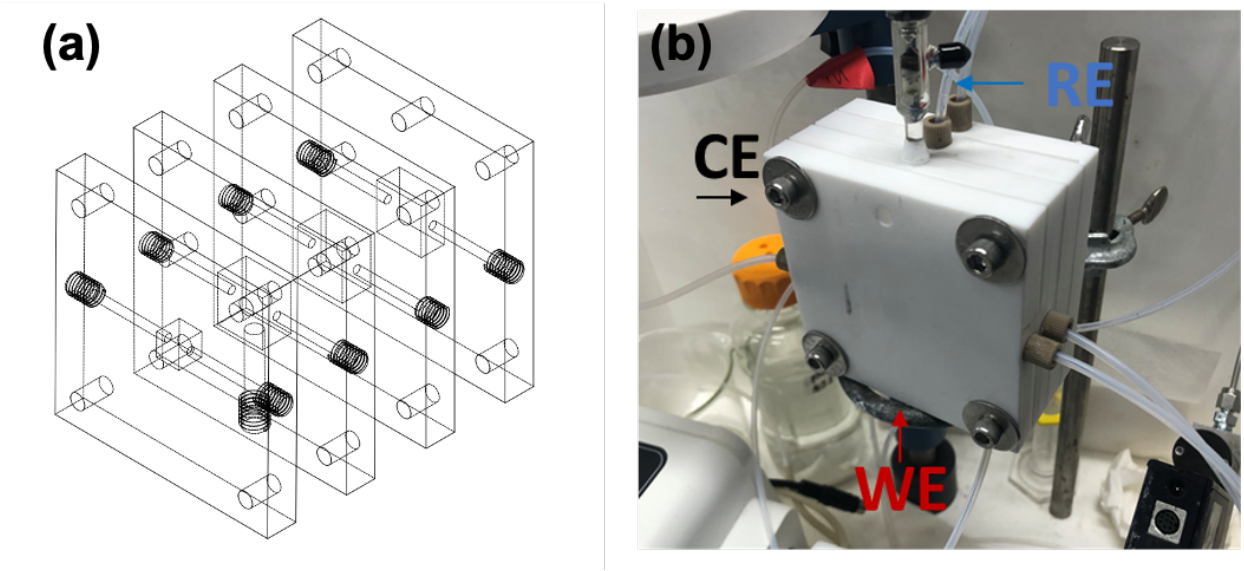

Figure S3: (a) Scheme and (b) photo of the three-compartment flow cell electrolyzer. RE = reference electrode, CE = counter electrode, and WE = working electrode.

Cell Performance

Experimental electrocatalysis data helped guide our selection of baseline parameters in our TEA. Fig. S4-S5 show the Faradaic efficiency versus current density for production of formate and methanol, respectively. While peak performance occurs at 150 mA/cm^2 and 100 mA/cm^2, respectively, due to economic benefits for higher current densities we use the performance at a current density of 200 mA/cm^2. Beyond this value, Faradaic efficiency begins to drop of more significantly. Quantitative ^{1}H-NMR spectra verifies production (Fig. S6).

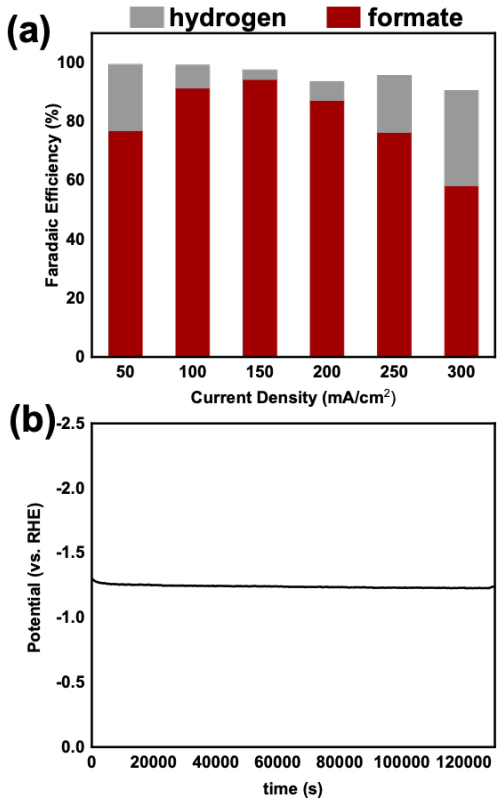

Figure S4: (a) Faradaic efficiency of CO_2-to-formate conversion at different current density with commercial bismuth catalysts (b) stability test of CO_2-to-formate catalysts under a constant current density of 150 mA/cm^2.

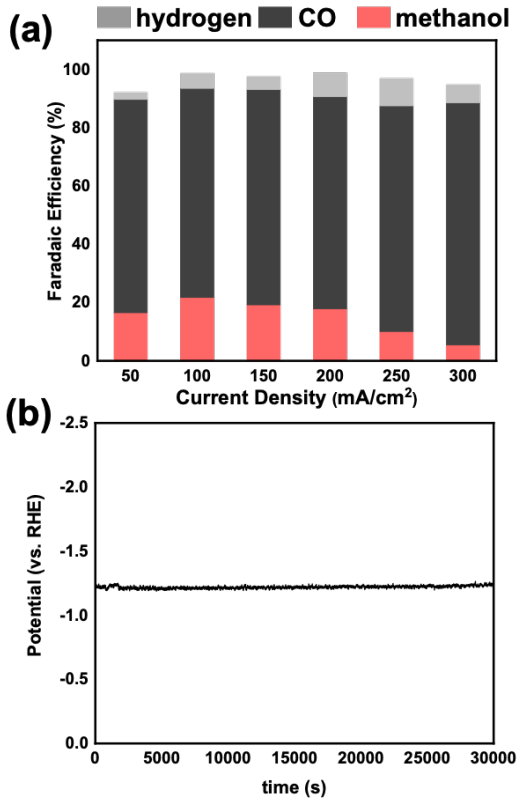

Figure S5: (a) Faradaic efficiency of CO_2-to-methanol conversion at different current density with modified cobalt phthalocyanine catalysts (b) stability test of CO_2-to-methanol catalysts under a constant current density of 100 mA/cm^2.

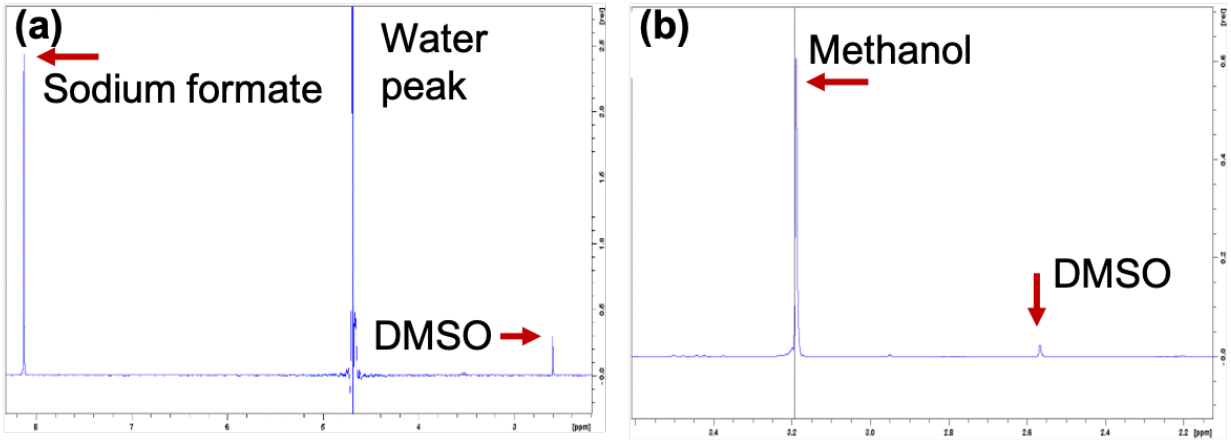

Figure S6: Quantitative ^{1}H-NMR spectra of (a) sodium formate and (b) methanol in post-reaction electrolyte with 5 mmol/L dimethyl sulfoxide as internal standard.

User Guidelines for Supplementary Spreadsheet

We sought to provide a user-friendly tool for researchers to evaluate their own scenarios with ease and provide an explicit model to follow. To this end, accompanying our work is a spreadsheet containing all pertinent calculations that went into our final model. Here, we include guidelines for the proper usage of our spreadsheet and a discussion of its features. This spreadsheet has 8 pages in total, discussed individually in the preceding sections.

Summary Table

The Summary Table page serves three purposes: to specify the desired scenario, to display the important process variables and design results, and to display the final economics. We colour code these sections using green, blue, and yellow, respectively, for simple differentiation.

Beginning with the scenario specification, the user has the option to chose from one of the 6 scenarios evaluated in our study or to specify their own process variables through a drop-down menu in cell C23. If one of the scenarios is chosen, the process variables are automatically set. However, if a user specified model is selected, the user has the option to input their desired process variables in cells C30:43. Once the scenario is set, the a quick calculation for the bioreactor design must be performed. This is done through a goal-seek, setting the target functions in cells C54:55 to 0 by varying the variables in cells D54:55.

Regardless of the scenario selected above, the user has the option to modify additional variables for sensitivity analysis in the section titled "Process Variables Input." All default values correspond to our baseline and are reflective of 2020 conditions. The baseline production capacity and operating days per year are given in cells H24:25. If these values are modified, calculations are scaled using appropriate scaling factors with the future technology, balanced scenario as the reference. For particular variables, the user is provided with a drop-down menu. The price of hydrogen gas, shown in cell H44, is calculated based on the user specification of green, blue, or grey hydrogen. For the carbon price, the user has the option to select a carbon price by jurisdiction or both user specification. If a jurisdiction carbon price is desired, this is set in cell H53. If user specification is desired, cell H53 is set to the "User Specified" option and the nominal value is input in cell H54. The final carbon price used by the model is reflected in cell H55. Similarly for electricity price, the user can select from a drop-down menu in cell H59 or input a user specified value in H60. Finally, the user can choose between electricity or natural gas as the source for steam generation. If electricity is chosen, the price of steam is calculated based in the specified electricity price; if natural gas is chosen, the price of steam is calculated based on the 2019 US average price of natural gas. [103] Beyond this section, no further user input is required for the spreadsheet.

With all variables set, the final process variables and key design features are displayed in cells C77:91 and cells H77:94, respectively. Furthermore, a simple, overall stoichiometric balance of the molar carbon in the process is provided in cells D100:I104. Economic results are displayed under the header "Key Economic Results" in column M. The major expenses are delineated by total capital costs, operating expenses, operating credits (sale of products), and overall operation cost. Below this, the final NPV is presented. The economics are calculated for four scenarios: the full process, the full process with HTL upgrade, the electrocatalysis subprocess, and the biocatalysis subprocess. For helpful visualisation, the NPV of each and subprocess is plotted, along with the capital and operating expenses for the full integrated process, broken down by major subprocess to better understand the cost drivers of the process. Finally, process emissions are given in cells M63:66, highlighting both the total emissions of operation over the plant lifetime and the total emissions avoided due to capture of the CO_2 that would otherwise be released into the air.

Carbon Flow

The Carbon Flow page follows the movement and conversion of the molar carbon at each major node in the process. The values are based on the user specified values input in the "Summary Table" page. Points where carbon enters or leaves the process are shaded in yellow, while internal streams are shade in blue. This allows for simple conversion calculations. These data can also be input directly into a Sankey diagram for better visualisation of the movement of the carbon through this process. Note, these molar quantities are calculated values based on the specified conversions, rather than explicit flow rates from the ASPEN Plus model. This leads to small deviations between these calculated values and our 6 scenarios. The carbon flow is presented for the full process, as well as the electrocatalysis and biocatalysis subprocesses. A reference table for the carbon stoichiometry is given at the bottom of the page for scaling purposes. This is shaded in grey.

Economics

The goal of this Economics page was to provide a fully explicit and representative economic model for our process. Here, a full NPV calculation is performed for the full process (Column A-V), electrocatalysis subprocess (Column W-AR), biocatalysis subprocess (Column AS-BN), and full process with additional HTL upgrade (Column BO-CH). Each individual unit and final cost are shaded in yellow, with all overall expenses shaded in green. Other data are shaded in blue. Similar expenses are grouped together and the total cost of these similar expenses are provided below each table. Outlined with every individual unit and cost are the unit specific factors that go into the final estimated cost. For example, capital expenses begin with a reference capacity and cost. In some cases, the capacity is also limited by some upper bound. The actual capacity for our model is provided by our ASPEN Plus model and scaled based on the user specified production capacity. Scaling factors and number of operators per unit are also input on a unit-by-unit basis. With this information, we can calculate the number of units required, total operators required, and installed cost of the equipment, indexed to 2019 USD, for each unit operation. For feedstock and material handling costs, the cost per unit is provided, along with the annual capacity of each species. This is similar for the product and operating credits.

Equipment operating costs are divided into four groups: electricity, cooling water, steam, and miscellaneous. For some units, quotes were given on a per unit basis and need to be scaled by the scaling factor and by the number of units. This is indicated in column C. For the units with operating costs that are not on a per unit basis, the costs are implicitly scaled through the design calculations. For each unit, costs are separated into these four groups and cells are left blank for units that do not use a particular operating expense. For example, for the methanol electrolyzer, operating costs for electricity and miscellaneous are provided, but are left blank for cooling water and steam since those utilities are not used. The total cost for each group are provided below the table. Moving on to administrative and maintenance costs, the operating labour is determined by the total number of operators required, which was calculated in the capital costs section. From this, hourly wages are converted to annual wages and added together. Supervision, laboratory, and overheads and administration are calculated based on a percentage of the total operating labour cost. Similarly, maintenance is computed based on a percentage of the total capital costs.

The final NPV calculation is adapted from the template provided by Jouny *et al.* [2] In the first table, the net capital expenses and net operating expenses are provided. For informational purposes, this net operating expense is also divided into operating expenses and operating credits. Income tax and interest rate are shown here, based on the user input from the "Summary Table" page. For the main calculation, up to 50 years are provided depending on the plant lifetime specified. In year one, the capital expenses and working capital are deducted, creating a negative cash flow and negative NPV. In the years following, cash flow is determined by depreciation, annual operating expenses, and income tax. The NPV is calculated based on this cash flow and the specified interest rate, reflecting the time value of money. We also implement the U.S. tax carryover credit, which provided tax breaks for companies that post negative profits in particular years. This tax break carries over into future years and allows a tax break on up to 80% of the total annual profit. This annual NPV calculation is repeated until the final year of the plant life, where any equipment in the plant that has salvage value is sold and the cumulative NPV at that point is the final NPV for our process. This NPV is reflected in cell C207 below this table. To understand the main cost drivers of each process, the capital and operating expenses are broken down into major subprocesses. These values are plotted on the "Summary Table" page.

Design Calculations

The Design Calculations page shows the explicit, step-by-step calculations that go into the design and costing of individual units. This is divided into 3 main sections: bioreactor calculations, electrocatalysis calculations, and additional equipment calculations. To help the user better understand the effect of major process variables on the design and economics, key input variables are italicised and key calculated variables are bolded throughout this page. The equations used for the design calculations are also provided in the Detailed Design Calculations section of this supplementary information.

In the bioreactor calculation section, the calculations are divided into two columns, one for the growth bioreactor and one for the accumulation bioreactor. First, reaction stoichiometry and heats of reaction are determined based on the specified biomass yields, PHB yields, and heats of combustion. This stoichiometry is then used to determine the mass balances around the bioreactors, which is also based on the specified production capacity. Heats of reaction are used subsequently to determine the amount of heat generated in each bioreactor. Next, the volume of the bioreactor is determined. Since a number of factors influence the required volume of the reactor, we evaluate the volume using three different methods. First, we evaluate a plug flow model to determine the

volume if the biomass is the volume-limiting factor. Second, we calculate the volume assuming the dilution rate is the volume limitation. Lastly, we assume the oxygen mass transfer to the liquid is volume-limiting and found the corresponding volume. The method that produces the largest volume is the volume limitation and that volume is used for the bioreactor design and economics. For the bioreactor design, we follow the procedure provided by Levett *et al.* [34] That is, the gas velocity and draft tube diameter are iteratively solved. Then, based on the calculated reactor dimensions, the cooling jacket, draft tube jacket, and cooling coils are sized.

Moving on to the electrocatalysis calculation section, we divide the methanol electrolyzer and formate electrolyzer into two different columns. User specified variables such as Faradaic efficiency and current density are paired with mass balance calculations to determine the power and size of each electrolyzer. These calculated values are used directly for the economic calculations of the electrolyzers. The component-by-component calculation of the electrolyzer cost is also explicitly provided with quoted prices from recent material purchases and a recent study. [66]

Additional unit design calculations are provided next. The rotary vacuum drum filter area is set by the allowable filter throughput. Pressure swing adsorption energy consumption is set by the energy requirement per unit of CO_2. For stirrer power calculations, we followed the procedure outlined by Chopey. [43] The volume is modelled assuming a square batch and a bulk velocity of 0.135 m/s is estimated based on density and viscosity of the liquid. Due to the low viscosity of water and resulting high Reynolds number, the pumping number becomes effectively independent of the Reynolds number and the pumping number is set by the impeller to tank diameter ratio. Lastly, we assume a pitched blade impeller with blades and a width to diameter ratio of 1/5. With an motor efficiency of 85%, we then calculated the required stirrer power. Nanofilter and microfilter power requirement are based on estimated power to flow rate ratios in literature. [50, 60] Finally, the steam requirement for electrocatalysis distillation needs to be estimated for user specified cases. To do this, we assume a constant ratio of CO_2 to water and CO_2 to $KHCO_3$ buffer and then perform an approximate mass balance around the distillation column.

Process Emissions

The Process Emissions page detail the total emissions and emissions on a per tonne of PHB basis for all materials, feedstocks, and utilities used in the specified scenario. To help guide the user, each source of emissions and the total emissions on a per tonne of PHB basis are highlighted in yellow. Emissions from each source are determined by using some reference value taken from literature and multiplied by the capacity as determined by the operating conditions input by the user. This value is further divided by the production capacity of PHB to arrive at a normalized value consistent with life cycle analysis protocol. [104, 105]

Emissions from the process are divided into three sections: materials for construction and decommissioning, feedstock, and utilities. Both the overall emissions and emissions on a per tonne of PHB basis are highlighted in green below at the bottom of the table. Following these three sections, the net lifetime and annual emissions are provided by summing up the contributions from these three sections. While emissions from materials for construction and decommissioning occur mainly at the beginning and end of the plant lifetime, these emissions are annualized to arrive at the calculated net annual emissions. Following this, the overall emissions if the plant was not built and the CO_2 emissions were released to the air is calculated using the capture rate of the integrated process. These values are provided in red. Sources for each reference value are provided at the bottom of the page.

ASPEN Material Balance Example

To aid with reproducing our calculations, we included the ASPEN Material Balance Example page with the full mass balance and operating conditions of each stream in our ASPEN Plus model for our future technology, balanced reference case. The process is divided into three main tables by major subprocess. Within these tables, species are grouped together based on its thermodynamics state. For each stream, mass flow rates are provided, with the temperature, pressure, and total flow rate given at the bottom of the table. The name for each stream corresponds to the labels in the process flow diagram that can be found under the mass balance tables. In this diagram, each stream and equipment is labelled clearly. The major subprocesses are also delineated by dashed lines. This page is not modified by any user input and is only for reference.

Scenarios Data

Where design calculations based on user input could not dynamically calculate new economics, variables directly from the ASPEN Plus model had to be provided. This Scenarios Data page holds this information in lookup

tables. Each lookup table contains seven rows, one for each scenario and one for the user specified scenario. For our scenarios, the values are taken directly from our Aspen model. For the user specified scenario, the values are scaled based on the future technology, balanced data. We divide the lookup data into three tables based on its relevance to the process or subprocess.

Market Variable Data

Market Variable Data holds the data required for the various drop-down menus in the "Summary Table" page. In the table under the head utility costs, different steam and electricity prices are provided based on the specified reference. Below the hydrogen costs header is the price of hydrogen from different sources. Finally, effective carbon prices by jurisdiction are provided, along with the type of carbon price for informational purposes.

Constants & Conversions

The Constants & Conversions page holds recurring constant variables necessary for performing our calculations, but would clutter the "Design Calculations" and "Economics" pages. These variables are grouped into five distinct groups: conversions, molecular weights, universal constant, miscellaneous, and electricity emissions data.

Detailed Design and Economic Calculations

Electrolyzer Power and Size Calculation

Electrolyzer Power:

$$P = \frac{zQ_{prod}FV}{\eta} \tag{12}$$

where P is the power, z is number of electrons required per mole of product, Q_{prod} is the molar flow rate of the product, F is Faraday's constant, V is the cell voltage, and η is the Faradaic efficiency.

Electrolyzer Area:

$$A = \frac{zQ_{prod}Fj}{\eta} \tag{13}$$

where A is the electrolyzer area and j is the current density.

Annual Catalyst Requirement:

$$C = A\rho_{cat}\frac{T}{t_{cat}} \tag{14}$$

where C is the required mass of catalyst per year, ρ_{cat} is the catalyst loading per unit area, T is the annual operating time, and t_{cat} is the catalyst lifetime.

Bioreactor Stoichiometry & Heat of Reaction

Stoichiometry of the biomass generation reaction is given in equation 5. The stoichiometric coefficients of methanol and formate, given by *a* and *b* respectively, are user specified. Then, the other coefficients can be calculated as follows:

$$\mathrm{g} = \mathrm{y}_{\mathrm{x,CH_3OH}}\frac{\mathrm{aM_{CH_3OH}}}{\mathrm{M}_x} + \mathrm{y}_{\mathrm{x,HCOO^-}}\frac{\mathrm{bM_{HCOO^-}}}{\mathrm{M}_x} \tag{15}$$

$$\mathrm{e} = \mathrm{a} + \mathrm{b} - 3.67\,\mathrm{g} \tag{16}$$

$$\mathrm{c} = 0.47\,\mathrm{g} \tag{17}$$

$$\mathrm{f} = \frac{4\,\mathrm{a} + \mathrm{b} + 3\,\mathrm{c} - 6.4\,\mathrm{g}}{2} \tag{18}$$

$$\mathrm{d} = \frac{-\mathrm{a} - 2\,\mathrm{b} + 2\,\mathrm{e} + \mathrm{f} + 2.2\,\mathrm{g}}{2} \tag{19}$$

where y is the yield and M is the molecular weight of the subscripted species. The heat generated during the reaction for biomass growth is related to the total amount of biomass produced:

$$\dot{Q}_{growth} = \Delta H_{r,x} F_x \tag{20}$$

where $\dot{Q}_{growth}$ is the heat rate generated in the growth reactor, $\Delta H_{r,x}$ is the heat of reaction for biomass generation, and F_x is the production rate of biomass.

Similarly, the stoichiometry of the PHB generation reaction is given in equation 6 and *a* and *b* are user specified. Then:

$$\mathrm{f} = \mathrm{y}_{\mathrm{PHB,CH_3OH}} \frac{\mathrm{aM_{CH_3OH}}}{\mathrm{M_{PHB}}} + \mathrm{y}_{\mathrm{PHB,HCOO^-}} \frac{\mathrm{bM_{HCOO^-}}}{\mathrm{M_{PHB}}} \tag{21}$$

$$\mathrm{d} = \mathrm{a} + \mathrm{b} - 4\,\mathrm{g} \tag{22}$$

$$\mathrm{e} = \frac{4\,\mathrm{a} + \mathrm{b} + 3\,\mathrm{c} - 6\,\mathrm{g}}{2} \tag{23}$$

$$\mathrm{c} = \frac{-\mathrm{a} - 2\,\mathrm{b} + 2\,\mathrm{e} + \mathrm{f} + 2\,\mathrm{g}}{2} \tag{24}$$

The heat generated during the reaction for PHB growth is related to the total amount of PHB produced and the total biomass:

$$\dot{Q}_{accum} = \Delta H_{r,PHB} F_{PHB} + \Delta H_{r,x,comb} F_x \tag{25}$$

where $\dot{Q}_{accum}$ is the heat rate generated in the accumulation reactor, $\Delta H_{r,PHB}$ is the heat of reaction for PHB generation, $\Delta H_{r,x,comb}$ is the heat of combustion for biomass and F_{PHB} is the production rate of PHB.

Bioreactor Cell Density

Since the substrate fed to the bioreactor is < 5 wt% in water, the cell density during growth and accumulation is dependent on the substrate concentration and the biomass/PHB yield, given by:

$$x = \sum_{s}^{n} y_{x,s} C_s \tag{26}$$

where x is the cell density, $y_{x,s}$ is the yield of product x, either biomass or PHB, from substrate s, either methanol or formate, and C_s is the concentration of the substrate s. Since formate and methanol can both be present during growth, the final cell density is the sum of growth on both substrates.

Bioreactor Volume Calculation

To determine the volume limiting factor for the bioreactors, we calculated volumes through three different methods. The calculation procedures for each are shown below.

Biomass Volume Limitation

Here, we followed the same procedure provided by Levett *et al.* in their SI. [34] For a more detailed description of the derivation, refer to this work. For both bioreactors, the required volume can be calculated using the following mass balance:

$$\begin{aligned} \mathrm{Accumulation} = \mathrm{Mass\,In} - \mathrm{Mass\,Out} \\ + \mathrm{Generation} - \mathrm{Consumption} \end{aligned} \tag{27}$$

In the case of the growth bioreactor, the operation is semi-batch with cycle that depends on the biomass yield - a function of the substrate composition. We specify 0.67 h for emptying. [34] Then, two mass balance equations are needed for the filling period and the emptying period. For the filling period, the equation is simplified as follows:

$$\begin{aligned}\text{Accumulation} &= \cancel{\text{Mass In}} - \cancel{\text{Mass Out}} \\ &\quad + \text{Generation} - \cancel{\text{Consumption}} \\ \frac{\mathrm{d(XV)}}{\mathrm{dt}} &= \mu \mathrm{XV} \\ \mathrm{XV} &= \mathrm{Be}^{\mu \mathrm{t}}\end{aligned} \tag{28}$$

where X is the biomass cell density, V is the volume of the reactor, and μ is the dilution rate. For the emptying period, the equation is simplifed as follows:

$$\begin{aligned}\text{Accumulation} &= \cancel{\text{Mass In}} - \text{Mass Out} \\ &\quad + \text{Generation} - \cancel{\text{Consumption}} \\ \frac{\mathrm{d(XV)}}{\mathrm{dt}} &= -\mathrm{F}_{x,out} + \mu \mathrm{XV} \\ \mathrm{XV} &= \mathrm{Ae}^{\mu \mathrm{t}} + \frac{\mathrm{F}_{x,out}}{\mu}\end{aligned} \tag{29}$$

where $\mathrm{F}_{x,out}$ is the flow rate of the biomass out of the growth bioreactor. Integration constants can be solved for using three boundary conditions:

1. At t = 0, XV = XV_0 (Minimum Volume)
2. At t = 8, XV = XV_0 (Minimum Volume)
3. At t = 7.33, XV = XV_0 + k = XV_{max} (Maximum Volume)

Once the integration constants are solved, the maximum volume is obtained by solving either equation at the end of the growth reactor filling period. For the accumulation bioreactor, the operation is batch with the same cycle time as the growth reactors. Then, equation 27 can be simplified to one equation to capture the bioreactor mass balance.

$$\begin{aligned}\text{Accumulation} &= \cancel{\text{Mass In}} - \cancel{\text{Mass Out}} \\ &\quad + \text{Generation} - \cancel{\text{Consumption}} \\ \frac{\mathrm{d(XV)}}{\mathrm{dt}} &= \mathrm{F}_{PHB,gen} \\ \mathrm{XV} &= \mathrm{F}_{PHB,gen}\mathrm{t} + \mathrm{C}\end{aligned} \tag{30}$$

where $\mathrm{F}_{PHB,gen}$ is the rate of PHB generation. The integration constant can be solved with the following boundary condition:

1. At t = 0, XV = $\mathrm{F}_{x,in}$ (Minimum Volume)

where $\mathrm{F}_{x,in}$ is the flow rate of biomass into the accumulation bioreactor. Then, the maximum volume is solved by setting t = 24 h.

Dilution Rate Limitation

Next, we calculate the required volume assuming the dilution rate is volume limiting. This can be calculated through the following equation:

$$V = \frac{F_{liq}}{D} \tag{31}$$

where F_{liq} is the flow rate of the liquid through the bioreactor and D is the dilution rate.

Oxygen Mass Transfer Limitation

For our approach, we assume oxygen mass transfer is the limiting component for the reactor performance and calculate the required volume under this assumption. To simplify mass transfer calculations, we use the following assumptions, based on Levett *et al.*'s similar mass transfer calculations:

1. Mass transfer of oxygen can be modelled by a plug flow model
2. Superficial gas velocity through the draft tube is constant
3. Mass transfer coefficient is constant
4. Henry's constant for O_2 is constant
5. Gases behave ideally

Our first step is to calculate the volumetric mass transfer, which is given by

$$N_{O_2} = k_L a(C^*_{L,O_2} - C_{L,O_2})_{LM} \tag{32}$$

where N_{O_2} is the volumetric mass trasnfer rate of oxygen, C_{L,O_2} is the actual concentration of oxygen in the liquid, C^*_{L,O_2} is the equilibrium concentration of oxygen in the liquid, k_La is the liquid side mass transfer coefficient, and (C^*_{L,O_2} - C_{L,O_2})$_{LM}$ is the log-mean concentration gradient. k_La can be calculated through the following equation derived by Akita and Yoshida. [106]

$$k_L a = 0.6 D_L^{0.5} \nu_L^{-0.12} (\gamma/\rho_L)^{-0.62} D^{0.17} g^{0.93} \varepsilon_G^{1.1} \tag{33}$$

where D_L is the liquid phase diffusivity, ν_L is the liquid kinematic viscosity, γ is the surface tension, ρ_L is the liquid density, D is the column diameter, g is gravitational constant, and ε_G is the gas holdup. All properties are assumed to be equivalent to water at the bioreactor temperature. Loq-mean concentration gradient can be calculated by:

$$(C^*_{L,O_2} - C_{L,O_2})_{LM} = \frac{(C^*_{L,O_2,in} - C_{L,O_2}) - (C^*_{L,O_2,out} - C_{L,O_2})}{\ln[\frac{(C^*_{L,O_2,in} - C_{L,O_2}}{(C^*_{L,O_2,out} - C_{L,O_2})}]} \tag{34}$$

$$C^*_{L,O_2} = H_{cc} C_{G,O_2} \tag{35}$$

$$C_{L,O_2} = 0.15 H_{cc} C_{G,O_2} \tag{36}$$

where H_{cc} is Henry's constant for oxygen, [107] and C_{G,O_2} is the concentration of oxygen in the gas phase. The factor of 0.15 refers to the assumption that the oxygen in the liquid is at 15% saturation. Once the volumetric mass transfer is determine, bioreactor volume is calculated using the required oxygen mass flow rate.

$$V = \frac{F_{O_2}}{N_{O_2}} \tag{37}$$

With three different calculated volumes, the final volume for each bioreactor will be the maximum of the three methods.

Bioreactor Dimensions

Calculation of the bioreactor dimensions begins by determining the working volume and total reactor volume:

$$V_{working} = V(1.0 + \varepsilon_G) \tag{38}$$

$$V_{total} = V(1.0 + \varepsilon_G)(1.0 + f_{hs}) \tag{39}$$

where f_{hs} is the bioreactor headspace. We specify a height to diameter ratio of *H=6D* based on similar bubble column bioreactors to calculate the diameter and subsequently, the height: [38]

$$D = (\frac{2}{3\pi} V_{total})^{0.33} \tag{40}$$

To calculate the diameter of the draft tube, an equation for the superficial gas velocity and for the draft tube diameter must be solved iteratively. These equations are given as:

$$U_G = \frac{H_L(H_{cc}k_La)}{\ln(\frac{C_{G,O_2,in}}{C_{G,O_2,out}})} \tag{41}$$

$$S_{draft} = \frac{Q_mRT}{H_LU_G\rho_{LG}}\ln[1+\frac{\rho_{LG}H_L}{P_H}] \tag{42}$$

where U_G is the superficial gas velocity, S_{draft} is the draft tube cross-sectional area, H_L is the bubble path length, equal to twice the working height of the bioreactor, Q_M is the gas flow rate, R is the universal gas constant, T is the reactor temperature, and P_H is the pressure in the bioreactor. With a self-consistent solution of these equations, the draft tube diameter can be calculated using S_{draft}.

Bioreactor Heat Transfer Design

Heat removal from the bioreactor is done using a reactor jacket, draft tube jacket, and cooling coils. The total heat flow was determined previously as $\dot{Q}_{growth}$ and $\dot{Q}_{accum}$. Then, the heat removal is given as:

$$\dot{Q}_{gen} = \dot{Q}_{jacket} + \dot{Q}_{draft} + \dot{Q}_{coils} \tag{43}$$

where $\dot{Q}_{jacket}$ is the heat removed through the cooling jacket, $\dot{Q}_{draft}$ is the heat removed through the draft tube jacket, and $\dot{Q}_{coils}$ is the heat removed through the cooling coils. $\dot{Q}_{jacket}$ and $\dot{Q}_{draft}$ are calculated directly from the previously determined bioreactor dimensions.

$$\dot{Q}_{jacket} = U_{jacket}A_rT_{LM} \tag{44}$$

$$\dot{Q}_{draft} = U_{jacket}A_{draft}T_{LM} \tag{45}$$

where U_{jacket} is the heat transfer coefficient of the cooling jacket, taken from Levett et al., [34] A_r is the heat transfer area of the bioreactor, A_{draft} is the heat transfer area of the draft tube, and T_{LM} is the log-mean temperature of the cooling water. The remaining heat is removed by the cooling coils, specified by the number of coils required. Using the coil diameter, spacing from the walls, and pitch provided by Levett et al., [34] the number of coils is calculated by:

$$N_{coils} = \frac{\dot{Q}_{coils}}{U_{coils}A_{coil}T_{LM}} \tag{46}$$

where N_{coils} is the number of coils, U_{coils} is the heat transfer coefficient of the cooling coils, and A_{coil} is the heat transfer area of an individual cooling coil. The height of the cooling coils can be calculated using the pitch of the coils and must be less than the working volume of the liquid.

Rotary Drum Filter Area Calculations

If filter capacity is specified, the filter size of a rotary vacuum drum filter is calculated by:

$$A_{filt} = \frac{C_{filt}}{F_{filt}} \tag{47}$$

where C_{filt} is the filter capacity per unit area and F_{filt} is the flow rate through the filter.

Pressure Swing Adsorption Energy Calculation

If energy consumption per unit of CO_2 is specified, total power is calculated by:

$$P_{PSA} = E_{PSA}F_{PSA,CO_2} \tag{48}$$

where E_{PSA} is the energy consumption per unit of CO_2 and F_{PSA,CO_2} is the mass flow rate of CO_2 through the PSA unit.

Stirred Vessel Stirrer Power Calculation

Stirrer power calculation is performed using the procedure outlined by Chopey. [43] First, the reactor volume is estimated as a square batch, yielding:

$$D = (\frac{4}{\pi}V)^{0.33} \tag{49}$$

Based on the properties of the liquid, we estimate a bulk velocity of the liquid. Then, the pumping capacity is:

$$F_{pump} = v_{bulk}\frac{\pi}{4}D^2 \tag{50}$$

where F_{pump} is the pumping capacity and v_{bulk} is the bulk velocity. The pumping number can be calculated using a pumping number versus Reynolds number plot. Due to the high Reynolds number of our liquid, pumping number is effectively independent of Reynolds number and the pumping number can be chosen based on impeller to reactor diameter ratio. Through this, the impeller speed is calculated:

$$N_{stir} = \frac{F_{pump}}{N_Q D^3} \tag{51}$$

where N_{stir} is the impeller speed and N_Q is the pumping number. Finally, stirrer power is estimated as:

$$P_{stir} = \frac{N_P \rho_L N_{stir}^3 D^5}{\eta} \tag{52}$$

where P_{stir} is the stirrer power, N_P is the power number, which is specified by the impeller geometry, and η is the motor efficiency.

Power Calculations

Power requirement for the disk stack centrifuge, rotary drum pressure filter, microfilter, and nanofilter is determined through a specified energy consumption per unit volume:

$$P_y = E_y F_y \tag{53}$$

where P_y is the power requirement, E_y is the energy consumption per unit volume, and F_y is the volumetric flow rate through the equipment. Here, y = cent, filt, micro, nano.

Net Present Value Calculation

Net present value of the process can be calculated through the following formula:

$$NPV(i,N) = \sum_{t=0}^{N} \frac{R_t}{(1+i)^t} \tag{54}$$

where NP(i,N) is the net present value understand a constant interest rate and plant life, N is the plant life, t is the year, R_t is the cash flow during year t, and i is the interest rate. Cash flow is the amount of money generated or spent by the company in a particular year. For our process, we delineate this by:

$$R_t = -R_{cap,t} - R_{work,t} + P_t - j(P_t - D_t - C_t) \tag{55}$$

where $R_{cap,t}$ is the cash flow for capital expenses in year t, $R_{work,t}$ is the cash flow for working capital in year t, P_t is the profit in year t, j is the tax rate, D_t is the depreciation in year t, and C_t is the tax credit that can be utilized in year t. In our scenarios, for $t = 0$, P_t, D_t , and C_t are equal to 0, while for $0 < t <$ N, $R_{cap,t}$ and $R_{work,t}$ are equal to 0. Tax credits can be accumulated during years when negative profit is recorded and can be used to get a tax break on up to 80% of a particular year's profit.

Steam Cost Calculation

Steam price, P_{steam}, of steam generated from electricity can be calculated through the following formula:

$$P_{steam} = P_{elec}(C_p \Delta T + \Delta H_{vap}) \tag{56}$$

where P_{elec} is the price of electricity per unit energy, C_p is the heat capacity of water, ΔT is the temperature difference between water at ambient conditions and steam at operating conditions (Table S4), and ΔH_{vap} is the enthalpy of vaporization at those conditions.
Similarly, the steam price of steam generated from natural has can be calculated through the following formula:

$$P_{steam} = P_{NG} \frac{(C_p \Delta T + \Delta H_{vap})}{\eta_{comb}} \tag{57}$$

where P_{NG} is the price of electricity per unit energy and η_{comb} is the combustion efficiency of natural gas to steam, which we take to be 85.7% based on the US Department of Energy. [108] At an electricity price of \$0.03/kWh and a natural gas price equal to the 2019 US average, [103] the resulting steam prices are \$0.022/kg and \$0.011/kg, respectively.

References

[1] De Luna, P. *et al.* What would it take for renewably powered electrosynthesis to displace petrochemical processes? *Science* **364**, eaav3506 (2019).

[2] Jouny, M., Luc, W. & Jiao, F. General techno-economic analysis of co2 electrolysis systems. *Industrial & Engineering Chemistry Research* **57**, 2165–2177 (2018).

[3] Taheri, A. & Berben, L. A. Making c–h bonds with co 2: production of formate by molecular electrocatalysts. *Chemical Communications* **52**, 1768–1777 (2016).

[4] Pérez-Fortes, M., Schöneberger, J. C., Boulamanti, A., Harrison, G. & Tzimas, E. Formic acid synthesis using co2 as raw material: Techno-economic and environmental evaluation and market potential. *international journal of hydrogen energy* **41**, 16444–16462 (2016).

[5] Haas, T., Krause, R., Weber, R., Demler, M. & Schmid, G. Technical photosynthesis involving co 2 electrolysis and fermentation. *Nature Catalysis* **1**, 32–39 (2018).

[6] Nangle, S. N., Sakimoto, K. K., Silver, P. A. & Nocera, D. G. Biological-inorganic hybrid systems as a generalized platform for chemical production. *Current opinion in chemical biology* **41**, 107–113 (2017).

[7] Yishai, O., Lindner, S. N., de la Cruz, J. G., Tenenboim, H. & Bar-Even, A. The formate bio-economy. *Current opinion in chemical biology* **35**, 1–9 (2016).

[8] Xia, C. *et al.* Continuous production of pure liquid fuel solutions via electrocatalytic co 2 reduction using solid-electrolyte devices. *Nature Energy* **4**, 776–785 (2019).

[9] Bushuyev, O. S. *et al.* What should we make with co2 and how can we make it? *Joule* **2**, 825–832 (2018).

[10] Nicholls, P. Formate as an inhibitor of cytochrome c oxidase. *Biochemical and biophysical research communications* **67**, 610–616 (1975).

[11] Korotkova, N. & Lidstrom, M. E. Connection between poly-β-hydroxybutyrate biosynthesis and growth on c1 and c2 compounds in the methylotroph methylobacterium extorquens am1. *Journal of Bacteriology* **183**, 1038 (2001).

[12] Hwang, H. W. *et al.* Two-stage bioconversion of carbon monoxide to biopolymers via formate as an intermediate. *Chemical Engineering Journal* **389**, 124394 (2020).

[13] Mitra, R., Xu, T., Xiang, H. & Han, J. Current developments on polyhydroxyalkanoates synthesis by using halophiles as a promising cell factory. *Microbial Cell Factories* **19**, 1–30 (2020).

[14] Rajan, K., Thomas, S., Gopanna, A. & Chavali, M. Polyhydroxybutyrate (phb): a standout biopolymer for environmental sustainability. *Handbook of Ecomaterials; Martínez, LMT, Kharissova, OV, Kharisov, BI, Eds* 1–23 (2018).

[15] Ritchie, H. & Roser, M. Plastic pollution. *Our World in Data* (2018).

[16] Albuquerque, P. B. & Malafaia, C. B. Perspectives on the production, structural characteristics and potential applications of bioplastics derived from polyhydroxyalkanoates. *International journal of biological macromolecules* **107**, 615–625 (2018).

[17] Zhu, Y., Albrecht, K. O., Elliott, D. C., Hallen, R. T. & Jones, S. B. Development of hydrothermal liquefaction and upgrading technologies for lipid-extracted algae conversion to liquid fuels. *Algal Research* **2**, 455–464 (2013).

[18] TerraGreen. Global waste — solvable problem as a renewable energy resource (2019). URL `https://medium.com/@support_61820/global-waste-solvable-problem-as-a-renewable-energy-resource-5d8f05cc1a7d`.

[19] Cho, E. J., Trinh, L. T. P., Song, Y., Lee, Y. G. & Bae, H.-J. Bioconversion of biomass waste into high value chemicals. *Bioresource technology* 122386 (2019).

[20] Perea-Moreno, M.-A., Samerón-Manzano, E. & Perea-Moreno, A.-J. Biomass as renewable energy: worldwide research trends. *Sustainability* **11**, 863 (2019).

[21] Jones, S. B. *et al.* Process design and economics for the conversion of algal biomass to hydrocarbons: whole algae hydrothermal liquefaction and upgrading. Tech. Rep., Pacific Northwest National Lab.(PNNL), Richland, WA (United States) (2014).

[22] Ou, L., Thilakaratne, R., Brown, R. C. & Wright, M. M. Techno-economic analysis of transportation fuels from defatted microalgae via hydrothermal liquefaction and hydroprocessing. *Biomass and Bioenergy* **72**, 45–54 (2015).

[23] Aspentech, A. P. V10. *Aspen Properties V10; Aspen Process Economic Analyzer V10* (2017).

[24] Max, S. P., Klaus, D. T. & Ronald, E. W. *Plant design and economics for chemical engineers* (McGraw-Hill Companies, 2003).

[25] Boutin, E. *et al.* Aqueous electrochemical reduction of carbon dioxide and carbon monoxide into methanol with cobalt phthalocyanine. *Angewandte Chemie International Edition* **58**, 16172–16176 (2019).

[26] Sen, S., Brown, S. M., Leonard, M. & Brushett, F. R. Electroreduction of carbon dioxide to formate at high current densities using tin and tin oxide gas diffusion electrodes. *Journal of Applied Electrochemistry* **49**, 917–928 (2019).

[27] Riboldi, L. & Bolland, O. Overview on pressure swing adsorption (psa) as co2 capture technology: state-of-the-art, limits and potentials. *Energy Procedia* **114**, 2390–2400 (2017).

[28] Wiheeb, A., Helwani, Z., Kim, J. & Othman, M. Pressure swing adsorption technologies for carbon dioxide capture. *Separation & Purification Reviews* **45**, 108–121 (2016).

[29] Ho, M. T., Allinson, G. W. & Wiley, D. E. Reducing the cost of co2 capture from flue gases using pressure swing adsorption. *Industrial & Engineering Chemistry Research* **47**, 4883–4890 (2008).

[30] Casas, N., Schell, J., Pini, R. & Mazzotti, M. Fixed bed adsorption of co 2/h 2 mixtures on activated carbon: experiments and modeling. *Adsorption* **18**, 143–161 (2012).

[31] Li, X. *et al.* Greenhouse gas emissions, energy efficiency, and cost of synthetic fuel production using electrochemical co2 conversion and the fischer–tropsch process. *Energy & Fuels* **30**, 5980–5989 (2016).

[32] Institute, M. Methanol technical data sheet for produced methanol (2020). URL `http://www.methanol.org/wp-content/uploads/2016/06/Methanol-Technical-Data-Sheet-1.pdf`.

[33] Dominguez-Ramos, A., Singh, B., Zhang, X., Hertwich, E. & Irabien, A. Global warming footprint of the electrochemical reduction of carbon dioxide to formate. *Journal of Cleaner Production* **104**, 148–155 (2015).

[34] Levett, I. *et al.* Techno-economic assessment of poly-3-hydroxybutyrate (phb) production from methane—the case for thermophilic bioprocessing. *Journal of Environmental Chemical Engineering* **4**, 3724–3733 (2016).

[35] Wendlandt, K.-D. *et al.* The potential of methane-oxidizing bacteria for applications in environmental biotechnology. *Engineering in Life Sciences* **10**, 87–102 (2010).

[36] Merchuk, J., Ben-Zvi, S. & Niranjan, K. Why use bubble-column bioreactors? *Trends in biotechnology* **12**, 501–511 (1994).

[37] Wendlandt, K.-D., Jechorek, M., Helm, J. & Stottmeister, U. Producing poly-3-hydroxybutyrate with a high molecular mass from methane. *Journal of biotechnology* **86**, 127–133 (2001).

[38] Humbird, D., Davis, R. & McMillan, J. Aeration costs in stirred-tank and bubble column bioreactors. *Biochemical engineering journal* **127**, 161–166 (2017).

[39] Cho, D. H., Jang, M. G. & Kim, Y. H. Formatotrophic production of poly-β-hydroxybutyric acid (phb) from methylobacterium sp. using formate as the sole carbon and energy source. *Korean Chemical Engineering Research* **54**, 719–721 (2016).

[40] Kalyuzhnaya, M. G. Unpublished data.

[41] Akberdin, I. R. *et al.* Methane utilization in methylomicrobium alcaliphilum 20z r: a systems approach. *Scientific reports* **8**, 1–13 (2018).

[42] Nagai, S. Mass and energy balances for microbial growth kinetics. In *Advances in Biochemical Engineering, Volume 11*, 49–83 (Springer, 1979).

[43] Chopey, N. P. *Handbook of chemical engineering calculations* (McGraw-Hill,, 2004).

[44] Narasimhan, K., Cearley, A. C., Gibson, M. S. & Welling, S. J. Process for the solvent-based extraction of polyhydroxyalkanoates from biomass (2008). US Patent 7,378,266.

[45] Muylaert, K., Bastiaens, L., Vandamme, D. & Gouveia, L. Harvesting of microalgae: overview of process options and their strengths and drawbacks. In *Microalgae-based biofuels and bioproducts*, 113–132 (Elsevier, 2017).

[46] (2020). Personal correspondence with Alfal Laval.

[47] (2020). Personal correspondence with GN Solids Control.

[48] (2020). Personal correspondence with Swiss Combi.

[49] (2020). Personal correspondence with Anderson Dahlen.

[50] Fasaei, F., Bitter, J., Slegers, P. & Van Boxtel, A. Techno-economic evaluation of microalgae harvesting and dewatering systems. *Algal Research* **31**, 347–362 (2018).

[51] Huttunen, M. *et al.* Real-time monitoring of the moisture content of filter cakes in vacuum filters by a novel soft sensor. *Separation and Purification Technology* **223**, 282–291 (2019).

[52] Shao, P. *et al.* Algae-dewatering using rotary drum vacuum filters: process modeling, simulation and techno-economics. *Chemical Engineering Journal* **268**, 67–75 (2015).

[53] Matches. Matches' process equipment cost estimates (2014).

[54] Gollakota, A., Kishore, N. & Gu, S. A review on hydrothermal liquefaction of biomass. *Renewable and Sustainable Energy Reviews* **81**, 1378–1392 (2018).

[55] Harrison, R. G., Todd, P., Rudge, S. R. & Petrides, D. P. *Bioseparations science and engineering* (Topics in Chemical Engineering, 2015).

[56] Green, D. W. & Perry, R. H. *Perry's Chemical Engineers' Handbook/edición Don W. Green y Robert H. Perry.* C 660.28 P47 2008. (2019).

[57] (2020). Personal correspondence with WesTech.

[58] Milledge, J. J. & Heaven, S. A review of the harvesting of micro-algae for biofuel production. *Reviews in Environmental Science and Bio/Technology* **12**, 165–178 (2013).

[59] (2020). Personal correspondence with AMS Membranes.

[60] Wafi, M. K. *et al.* Nanofiltration as a cost-saving desalination process. *SN Applied Sciences* **1**, 751 (2019).

[61] Yang, D. *et al.* Selective electroreduction of carbon dioxide to methanol on copper selenide nanocatalysts. *Nature communications* **10**, 1–9 (2019).

[62] Fan, L., Xia, C., Zhu, P., Lu, Y. & Wang, H. Electrochemical co 2 reduction to high-concentration pure formic acid solutions in an all-solid-state reactor. *Nature communications* **11**, 1–9 (2020).

[63] Belkhelfa, S. *et al.* Continuous culture adaptation of methylobacterium extorquens am1 and tk 0001 to very high methanol concentrations. *Frontiers in microbiology* **10**, 1313 (2019).

[64] Peyraud, R. *et al.* Genome-scale reconstruction and system level investigation of the metabolic network of methylobacterium extorquens am1. *BMC systems biology* **5**, 1–22 (2011).

[65] Jenkins, S. Economic indicators: Cepci. *Chemical Engineering* **24** (2020).

[66] Verma, S., Kim, B., Jhong, H.-R. M., Ma, S. & Kenis, P. J. A gross-margin model for defining technoeconomic benchmarks in the electroreduction of co2. *ChemSusChem* **9**, 1972–1979 (2016).

[67] Remer, D. S. & Chai, L. H. Process equipment, cost scale-up (1993).

[68] Ulrich, G. D. *et al. A guide to chemical engineering process design and economics* (Wiley New York, 1984).

[69] DeSantis, D., James, B. D. & Saur, G. Current hydrogen production from central pem electrolysis. Tech. Rep., National Renewable Energy Lab.(NREL), Golden, CO (United States) (2019).

[70] of Labor Statistics, U. B. Occupational employment statistics: Chemical plant and system operators (2017). URL `https://www.bls.gov/oes/2017/may/oes518091.htm`.

[71] Ewing, R. Downward price pressure on ammonia remains for june loadings (2020). URL `https://www.icis.com/explore/resources/news/2020/05/29/10513459/downward-price-pressure-on-ammonia-remains-for-june-loadings`. Based on 6 month average.

[72] ECHEMI. Acetone price analysis (2020). URL `https://www.echemi.com/productsInformation/pid_Rock3929-acetone.html`. Based on 6 month average.

[73] Molbase. Cas no.3317-67-7 cobalt phthalocyanine (2020). URL `http://www.molbase.com/en/cas-3317-67-7.html`.

[74] Nano, S. Tin oxide nanoparticles/nanopowder (2020). URL `https://www.ssnano.com/inc/sdetail/tin_oxide_nanoparticles__nanopowder___sno2___99_9____50_70_nm_/235`.

[75] IEA. The future of hydrogen. Tech. Rep., International Energy Agency, France (2019).

[76] Clippinger, J. N. & Davis, R. E. Techno-economic analysis for the production of algal biomass via closed photobioreactors: future cost potential evaluated across a range of cultivation system designs. Tech. Rep., National Renewable Energy Lab.(NREL), Golden, CO (United States) (2019).

[77] Stiglitz, J. E. *et al.* Report of the high-level commission on carbon prices (2017).

[78] Institute, M. Methanol price and supply/demand (2020). URL `https://www.methanol.org/methanol-price-supply-demand/`. Based on 6 month average.

[79] ECHEMI. Sodium formate price analysis (2020). URL `https://www.echemi.com/productsInformation/pd20150901132-sodium-formate.html`. Based on 6 month average.

[80] EIA. Weekly retail gasoline and diesel prices (2020). URL https://www.eia.gov/dnav/pet/pet_pri_gnd_dcus_nus_a.htm. Based on 2019 average.

[81] Ulrich, G. D. & Vasudevan, P. T. *Chemical engineering process design and economics: a practical guide* (Process Publishing, 2004).

[82] IEA. Electricity information (2020). Based on 2019 average.

[83] EIA. Electric power monthly (2020). URL https://www.eia.gov/electricity/monthly/epm_table_grapher.php?t=epmt_5_6_a. Based on 2019 average.

[84] IRENA. How falling costs make renewable a cost-effective investment (2020).

[85] IRENA. Future of solar photovoltaic: Deployment, investment, technology, grid integration, and socio-economic aspects (2019).

[86] Haegel, N. M. *et al.* Terawatt-scale photovoltaics: Trajectories and challenges. *Science* **356**, 141–143 (2017).

[87] Malkhandi, S. & Yeo, B. S. Electrochemical conversion of carbon dioxide to high value chemicals using gas-diffusion electrodes. *Current Opinion in Chemical Engineering* **26**, 112–121 (2019).

[88] Liu, Y., Li, F., Zhang, X. & Ji, X. Recent progress on electrochemical reduction of co2 to methanol. *Current Opinion in Green and Sustainable Chemistry* **23**, 10–17 (2020).

[89] Khosravi-Darani, K., Mokhtari, Z.-B., Amai, T. & Tanaka, K. Microbial production of poly (hydroxybutyrate) from c 1 carbon sources. *Applied microbiology and biotechnology* **97**, 1407–1424 (2013).

[90] Wernet, G. *et al.* The ecoinvent database version 3 (part i): overview and methodology. *The International Journal of Life Cycle Assessment* **21**, 1218–1230 (2016).

[91] Johnston, A. H. & Karanfil, T. Calculating the greenhouse gas emissions of water utilities. *Journal-American Water Works Association* **105**, E363–E371 (2013).

[92] Agency, U. S. E. P. Ap 42, fifth edition, volume i, chapter 8: Inorganic chemical industry. Tech. Rep., United States Environmental Protection Agency (1993).

[93] Amelio, A., Genduso, G., Vreysen, S., Luis, P. & Van der Bruggen, B. Guidelines based on life cycle assessment for solvent selection during the process design and evaluation of treatment alternatives. *Green Chemistry* **16**, 3045–3063 (2014).

[94] Nuss, P. & Eckelman, M. J. Life cycle assessment of metals: a scientific synthesis. *PloS one* **9**, e101298 (2014).

[95] Asdrubali, F., Baldinelli, G., D'Alessandro, F. & Scrucca, F. Life cycle assessment of electricity production from renewable energies: Review and results harmonization. *Renewable and Sustainable Energy Reviews* **42**, 1113–1122 (2015).

[96] Ritchie, H. & Roser, M. Renewable energy. our world in data (2020).

[97] Agency, U. S. E. P. Inventory of u.s. greenhouse gas emissions and sinks: 1990-2018. annex 2 (methodology for estimating co2 emissions from fossil fuel combustion), table a-43 (2020). URL https://www.epa.gov/energy/greenhouse-gases-equivalencies-calculator-calculations-and-references.

[98] Nicholson, S. R., Rorrer, N. A., Carpenter, A. C. & Beckham, G. T. Manufacturing energy and greenhouse gas emissions associated with plastics consumption. *Joule* **5**, 673–686 (2021).

[99] Mostafa, Y. S. *et al.* Bioplastic (poly-3-hydroxybutyrate) production by the marine bacterium pseudodonghicola xiamenensis through date syrup valorization and structural assessment of the biopolymer. *Scientific Reports* **10**, 1–13 (2020).

[100] Incorporated, B. Global polypropylene market forecast hurt in 2020 but still strong, says beroe inc (2021). URL https://www.prnewswire.com/news-releases/global-polypropylene-market-forecast-hurt-in-2020-but-still-strong-says-beroe-inc-301259469.html.

[101] Wu, Y., Jiang, Z., Lu, X., Liang, Y. & Wang, H. Domino electroreduction of co 2 to methanol on a molecular catalyst. *Nature* **575**, 639–642 (2019).

[102] Huang, N. *et al.* A stable and conductive metallophthalocyanine framework for electrocatalytic carbon dioxide reduction in water. *Angewandte Chemie International Edition* **59**, 16587–16593 (2020).

[103] EIA. Natural gas monthly (2020). Based on 2019 average.

[104] Rebitzer, G. *et al.* Life cycle assessment: Part 1: Framework, goal and scope definition, inventory analysis, and applications. *Environment international* **30**, 701–720 (2004).

[105] Pennington, D. W. *et al.* Life cycle assessment part 2: Current impact assessment practice. *Environment international* **30**, 721–739 (2004).

[106] Akita, K. & Yoshida, F. Gas holdup and volumetric mass transfer coefficient in bubble columns. effects of liquid properties. *Industrial & Engineering Chemistry Process Design and Development* **12**, 76–80 (1973).

[107] Sander, R. Compilation of henry's law constants (version 4.0) for water as solvent. *Atmos. Chem. Phys* **15**, 4399–4981 (2015).

[108] DOE, U. Benchmark the fuel cost of steam generation. Tech. Rep., United States Department of Energy (2012). URL `https://www.energy.gov/sites/prod/files/2014/05/f16/steam15_benchmark.pdf`.